Canadian Journal of Research

Issued by THE NATIONAL RESEARCH COUNCIL OF CANADA

VOL. 26, SEC. F. DECEMBER, 1948 NUMBER 12

NONISOTHERMAL PRESSURE DROP FOR A GAS[1]

BY NORMAN EPSTEIN[2] AND JOHN B. PHILLIPS[3]

Abstract

An equation for calculating the pressure drop in gas flow accompanied by large temperature change, derived from the differential form of the Bernoulli theorem combined with the heat transfer rate equation, was examined experimentally. Heating runs were made in the Reynolds number range 6000 to 15,000, for air flowing through a single horizontal ¼ in. standard steel pipe with steam jacket. The pressure drops calculated from the proposed equation were found to agree very closely with the observed experimental values. The method of evaluating pressure drop for turbulent nonisothermal flow by assuming isothermal conditions at a temperature midway between the surface temperature and the mean bulk temperature of the fluid, first developed by McAdams for certain oils, was also tested for a number of selected runs. This method was found to be as accurate as the previous one, and to have the advantage of being less cumbersome in application.

Introduction

The problem of fluid friction for isothermal flow in round pipes has been very thoroughly investigated as compared with that for nonisothermal flow. The friction factor f is defined (16) by the familiar differential form of Bernoulli's theorem:

$$dx + vdp + \frac{udu}{g} + \frac{2fu^2dL}{Dg} = 0 ,$$

where the symbols have the meanings listed in the nomenclature. For streamline or viscous flow, the law established by Hagen (4) in 1839 and Poiseuille (11) in 1842 has been many times confirmed if the calming length were at least 30 diameters (13). In terms of the present symbols it is

$$f = \frac{16}{Re} .$$

For turbulent flow, the accepted friction factor plots for smooth tubes and clean commercial iron and steel pipes, respectively, are those of Drew, Koo, and McAdams (3), the results of an all-embracing literature survey. In the case of corroded or tuberculated commercial pipes, however, especially those

[1] *Manuscript received in original form June 2, 1948, and, as revised, September 8, 1948. Contribution from the Department of Chemical Engineering, McGill University, Montreal, Que.*

[2] *Lecturer.*

[3] *Professor.*

of smaller diameter as in the present investigation, values of f are considerably greater than those read from the aforementioned plots (2, 7), and a roughness factor must be applied.

Recorded research on nonisothermal fluid friction has so far been restricted to liquids only, particularly oils. Available data (1, 5, 6, 18) all indicate that for a given value of the Reynolds number based on a viscosity evaluated at the mean bulk temperature of the oil, the friction factor during heating is less than in isothermal flow, while, for cooling, the friction factor is greater, especially when the flow is in the viscous region. These results have been reconciled with the isothermal friction factor plots by evaluating the viscosity at a temperature

$$t' = t + (t_s - t)/4$$

for streamline flow, and

$$t' = t + (t_s - t)/2$$

for turbulent flow (10). Another successful correlation, based on the same data as well as other data (14), involves multiplying the friction factor for nonisothermal flow by a correction ψ, where

$$\psi = 1.1\ (\mu/\mu_s)^{0.25}$$

for viscous flow, and

$$\psi = 1.0\ (\mu/\mu_s)^{0.14}$$

in the turbulent region (15). In a study of the cooling of water in a brass tube (12), it was found that nonisothermal friction factor data fall in line with isothermal data when the viscosity term in the Reynolds number is evaluated at the mean wall temperature. A complex triple integral expression (8, pp. 571-577) relating isothermal and nonisothermal pressure drop for viscous flow has been verified for water and an oil (9).

In the case of nonisothermal flow of gases, since the variation of viscosity with temperature is small as compared with that of liquids, the problem of finding the correct temperature at which to evaluate Re in order to use isothermal friction data is of minor consequence (6). But the compressible property of gases introduces the new problem of how to evaluate correctly the changing specific volume, which occurs explicitly in the pressure head term of Bernoulli's equation, and implicitly in the velocity head and Fanning friction terms. Where the specific volume does not vary greatly, the Bernoulli differential equation may be integrated with little error by using an average value of v (17). However, this is not applicable to cases where the variation of v is large.

A method of integrating the differential form of the Bernoulli equation by assuming that the pressure change is small compared with the temperature change was developed by J. H. Holden and W. Gauvin of McGill University in 1943, using simple thermodynamic relations. The present investigation was undertaken for the purpose of testing this formula within the lower turbulent range for the heating of air.

Formula Derivation

The energy balance for the flow of gases has been developed as follows (17). The differential form of Bernoulli's equation is given by

$$vdp + \frac{udu}{g} + \frac{2fu^2dL}{Dg} = 0 \tag{1}$$

for a horizontal conduit.

Converting from local velocity u to average velocity V, since $V/v = G$, and $dV = Gdv$ for steady flow,

$$vdp + \frac{G^2vdv}{g} + \frac{2fG^2v^2dL}{Dg} = 0 .$$

Multiplying through by p/v,

$$pdp + \frac{G^2pdv}{g} + \frac{2fG^2pvdL}{Dg} = 0 .$$

Substituting the ideal gas law relation $p = NRT/v$,

$$pdp + \frac{G^2NRTdv}{vg} + \frac{2fG^2NRTdL}{Dg} = 0 . \tag{2}$$

For isothermal flow, this equation can be integrated directly to the familiar form

$$\frac{p_1^2 - p_2^2}{2} = \frac{NRTG^2}{g}\left(\ln\frac{p_1}{p_2} + \frac{2fL}{D}\right) . \tag{3}$$

For nonisothermal flow, Equation (2) is rearranged:

$$pdp + \frac{NRTG^2}{g} \cdot \frac{dv}{v} = -\frac{2NRTfG^2dL}{Dg} .$$

Since the Reynolds number does not vary greatly, f may be considered constant, and an average value used. Holden and Gauvin considered that if the change in pressure is relatively small compared with the change in temperature, then dT/T may be substituted for dv/v, and this leads to an expression that could be integrated:

$$pdp + \frac{NRG^2dT}{g} = -\frac{2NRTfG^2dL}{Dg} .$$

In order to integrate this equation T must be expressed as a function of L. By a heat balance on a differential length dL,

$$G\pi D^2cdT/4 = h\pi D(t_s - T)dL ,$$

or

$$\frac{dT}{t_s - T} = \frac{4hdL}{DGc} .$$

Integrating between $T = T_1$ at $L = 0$, and any value T and L,

$$\ln \frac{t_s - T_1}{t_s - T} = \frac{4hL}{DGc} = \alpha L ,$$

where α replaces $4h/DGc$.

Therefore $$\frac{t_s - T_1}{t_s - T} = e^{\alpha L}$$

or $$(t_s - T_1)e^{-\alpha L} = t_s - T .$$

Rearranging, $$T = t_s - (t_s - T_1)e^{-\alpha L} .$$

Substituting in the energy balance,

$$pdp + \frac{NRG^2dT}{g} = - \frac{2NRfG^2}{Dg}\left[t_s - (t_s - T_1)e^{-\alpha L}\right] dL . \qquad (4)$$

Integrating between the limits p_1, T_1, 0, and p_2, T_2, L,

$$\frac{p_2^2 - p_1^2}{2} + \frac{NRG^2(T_2 - T_1)}{g} = - \frac{2NRfG^2}{Dg}\left[t_sL + \frac{(t_s - T_1)e^{-\alpha L}}{\alpha}\right]_0^L$$

$$= - \frac{2NRfG^2}{Dg}\left(t_sL + \frac{t_s - T_1}{\alpha e^{\alpha L}} - \frac{t_s - T_1}{\alpha}\right)$$

$$= + \frac{2NRfG^2}{Dg}\left(\frac{t_s - T_1}{\alpha} - \frac{t_s - T_1}{\alpha e^{\alpha L}} - t_sL\right) .$$

For a rough pipe, f must be modified by the roughness factor X, and the final expression becomes

$$\frac{p_2^2 - p_1^2}{2} + \frac{NRG^2(T_2 - T_1)}{g} = \frac{2NRfXG^2}{Dg}\left(\frac{t_s - T_1}{\alpha} - \frac{t_s - T_1}{\alpha e^{\alpha L}} - t_sL\right) . \qquad (5)$$

Description of Apparatus

A diagrammatic sketch of the apparatus used in this investigation is shown in Fig. 1. A steady flow of air was provided by means of a rotary compressor, belt-driven by a $\frac{1}{4}$ hp. motor. The air rate was controlled by means of a by-pass valve to the atmosphere and was measured by an orifice. The orifice drop was read on a water manometer and the orifice upstream pressure on a mercury manometer. The steam pressure was regulated by means of a globe valve and measured on a Bourdon gauge. A calming length of 50 diameters preceded the heating section ($L = 5.0$ ft.), which consisted of a $\frac{1}{4}$ in. standard steel pipe ($D = 0.0303$ ft.) inside a $\frac{3}{4}$ in. standard steel steam jacket, with magnesia–asbestos ("Aircell") lagging ($\frac{7}{8}$ in. thick) on the outside. Thermometers were placed at the inlet and outlet of the heating section, and the pressure drop across this section was read on a mercury manometer.

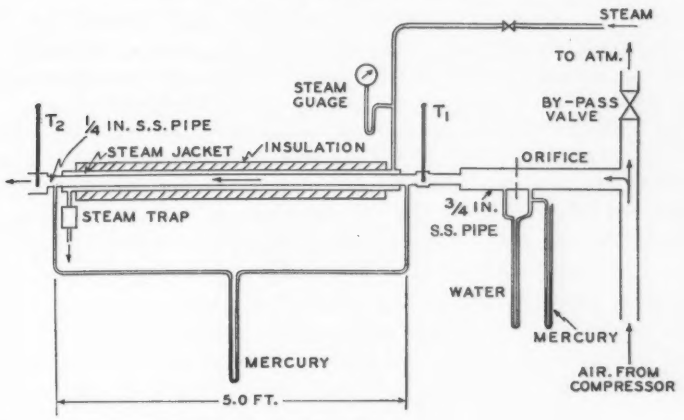

FIG. 1.

Experimental Procedure

In order to determine the roughness factor and its variation with mass velocity, a set of 10 isothermal trials were made initially throughout the entire velocity range of the apparatus.

Four sets of 10 heating runs each were then made at steam pressures of 5, 10, 15, and 20 p.s.i. gauge, respectively. Each run was carried on for 20 min. after ensuring that thermal equilibrium had been reached, and readings of orifice drop and pressure, inlet, and outlet temperatures, and pressure drop, were recorded at five-minute intervals.

The mean values of the above readings for each run were used in Equation (5) to calculate the pressure drop. The temperature corresponding to saturated steam at the recorded steam pressure was taken as the inside surface temperature (t_s) of the conduit, as calculations showed that the air film was controlling. The calculated and observed pressure drops for the 40 runs are given in Table I.

TABLE I

COMPARISON OF CALCULATED AND OBSERVED PRESSURE DROPS

t_s, ° F. abs.	Run No.	G, lb./(sec.) (ft.)^2	$\Delta p_{calc.}$ cm. Hg	$\Delta p_{obs.}$ cm. Hg	Dev'n., %
687.1	1	2.92	1.36	1.44	−5.55
	2	3.65	2.08	2.17	−4.15
	3	4.05	2.55	2.59	−1.55
	4	4.64	3.32	3.34	−0.60
	5	4.91	3.65	3.72	−1.88
	6	5.30	4.25	4.29	−0.93
	7	5.60	4.66	4.67	−0.21
	8	5.97	5.26	5.32	−1.13
	9	6.25	5.75	5.70	+0.87
	10	6.40	6.00	5.98	+0.33

TABLE I—*Concluded*

COMPARISON OF CALCULATED AND OBSERVED PRESSURE DROPS—*Concluded*

t_s, ° F. abs.	Run No.	G, lb./(sec.) (ft.)^2	$\Delta p_{calc.}$ cm. Hg	$\Delta p_{obs.}$ cm. Hg	Dev'n., %
699.4	11	2.74	1.23	1.30	−5.38
	12	4.08	2.60	2.71	−4.05
	13	4.46	3.13	3.15	−0.63
	14	5.10	3.95	4.01	−1.49
	15	5.20	4.14	4.12	+0.48
	16	5.71	4.99	5.04	−0.99
	17	5.94	5.26	5.31	−0.94
	18	6.14	5.63	5.66	−0.53
	19	6.26	5.94	5.91	+0.51
	20	6.45	6.20	6.08	+1.97
709.8	21	2.96	1.43	1.51	−5.30
	22	3.80	2.30	2.44	−5.98
	23	3.95	2.45	2.60	−5.77
	24	4.45	3.12	3.21	−2.80
	25	4.91	3.74	3.87	−3.36
	26	5.36	4.45	4.57	−2.62
	27	5.75	5.05	5.16	−2.13
	28	6.06	5.56	5.61	−0.89
	29	6.28	5.78	6.00	−3.67
	30	6.51	6.37	6.37	0.00
718.8	31	2.86	1.34	1.36	−1.47
	32	3.51	1.99	2.02	−1.48
	33	3.95	2.52	2.49	+1.20
	34	4.51	3.22	3.24	−0.62
	35	4.91	3.76	3.82	−1.57
	36	5.42	4.58	4.62	−0.87
	37	5.53	4.66	4.79	−2.71
	38	5.91	5.33	5.43	−1.84
	39	6.08	5.64	5.70	−1.05
	40	6.43	6.25	6.29	−0.64

Discussion

The results indicate substantial agreement between calculated and observed pressure drops for the entire range of velocity and steam pressure used in the investigation. Although the deviation range of −6% to + 2% is within the possible experimental error, with the percentage deviations in general numerically decreasing with increase in manometer readings as would be expected, the preponderance of negative over positive deviations may not be merely a coincidence, and there were no apparent apparatus defects to account for it. The probable explanation lies in the fact that the calculations for these runs were made using a friction factor based on the mean air temperature, rather than a mean of the friction factors at the inlet and outlet of the heating section. The latter procedure would have resulted in a slightly higher value of f in each case, hence a slightly higher calculated pressure drop, and therefore a slightly higher (algebraically, not numerically) deviation. This contention was actually verified for a few sample runs. There would thus have been a more symmetrical distribution of positive and negative errors.

It should be noted that, from the derivation of Equation (5), this relation is applicable only when the pressure change is relatively small compared with the temperature change, and this disparity is often the case in industrial practice, e.g., in air heaters and coolers, gas preheaters, etc. Although the present experiment has verified this equation only for the heating of air in the lower turbulent region (Re = 6000 to 15,000), there appears to be nothing in the derivation that would preclude its applicability to the heating or cooling of any reasonably "ideal" gas in either the viscous flow or higher turbulent ranges, if the above condition is assumed to hold. However, it is not valid to make such a generalization without further experimentation.

It was deemed of interest to calculate the pressure drop for a few of the runs in this investigation by means of the familiar relation (Equation (3)) for isothermal pressure drop for a gas. Since in the present case the pressure change is relatively small, and f must be modified by the roughness factor X, the above equation reduces to

$$\frac{p_1^2 - p_2^2}{2} = \frac{2NRt'G^2fLX}{gD},$$

where $t' = t + (t_s - t)/2$, and f is evaluated at t'. The runs selected for this calculation were those at the lowest and highest mass velocities for each of the four steam pressures. The results are tabulated in Table II.

TABLE II

EVALUATION OF DATA USING "ISOTHERMAL" EQUATION 3

t_s, °F. abs.	Run No.	G, lb./(sec.) (ft.)^2	t' ° F. abs.	$\Delta p_{calc.}$ cm. Hg	$\Delta p_{obs.}$ cm. Hg	% Dev'n. Eq'n. (3)	% Dev'n. Eq'n. (5)
687.1	1	2.92	646.0	1.41	1.44	−2.08	−5.55
	10	6.40	649.5	6.10	5.98	+2.01	+0.33
699.4	11	2.74	653.6	1.27	1.30	−2.31	−5.38
	20	6.45	656.8	6.30	6.08	+3.62	+1.97
709.8	21	2.96	661.0	1.48	1.51	−1.99	−5.30
	30	6.51	664.3	6.49	6.37	+1.88	0.00
718.8	31	2.86	668.8	1.40	1.36	+2.86	−1.47
	40	6.43	669.5	6.41	6.29	+1.91	−0.64

The calculated results are therefore generally as accurate as those obtained using the much more complex relation in Equation (5). This semiempirical method seemingly would be more useful in practice, at least for the lower turbulent range.

The fact that the deviations using Equation (3) are consistently greater algebraically than the corresponding deviations using Equation (5), and that there is a more symmetrical distribution of positive and negative errors in

the case of the former, supports the contention that the uneven distribution of deviations using the latter formula is not due to divergence of the actual apparatus from an ideal system.

Conclusions

Equation (5), developed by Holden and Gauvin, successfully predicts, with reasonable accuracy, the pressure drop for the flow of a gas in a horizontal pipe accompanied by a large temperature change, within the lower turbulent region (Re = 6000 to 15,000).

The method of evaluating data for turbulent nonisothermal runs by assuming that these runs occur isothermally at a temperature midway between the surface temperature and the mean bulk temperature of the fluid, a method first developed by McAdams for certain oils, is as accurate as the method of Holden and Gauvin in predicting nonisothermal pressure drop or a gas flowing in a horizontal pipe, and has the advantage for industrial design purposes of being much less cumbersome.

Definition of Symbols

c = heat capacity of gas, B.t.u./(lb.) (° F.),

D = inside diameter of conduit, ft.,

f = friction factor in Fanning equation, dimensionless,

G = mass velocity of gas, lb./(sec.) (ft.)^2,

g = acceleration due to gravity, 32.2 ft./sec.^{2},

h = gas film coefficient of heat transfer obtained from a heat balance on the heating section, B.t.u./(sec.) (ft.)^2 (° F. abs.),

L = heating (or cooling) length of conduit, ft.,

N = reciprocal of molecular weight of gas, lb-moles/lb.,

p = fluid pressure, lb./ft.^{2},

p_1 = inlet pressure of gas, lb./ft.^{2},

p_2 = outlet pressure of gas, lb./ft.^{2},

$\Delta p_{calc.}$ = calculated pressure drop, cm. Hg.

$$= \frac{(p_1 - p_2)\ 76}{(144)\ (14.7)}.$$

$\Delta p_{obs.}$ = observed pressure drop, cm. Hg.,

p_s = steam gauge pressure, lb./in.^{2},

R = ideal gas law constant, 1543 ft.-lb./(lb-moles) (° F. abs.),

Re = Reynolds number, dimensionless, = $DG/0.000672\ \mu$,

T = gas temperature, (° F. abs.),

T_1 = inlet temperature of gas, (° F. abs.),

T_2 = outlet temperature of gas, (° F. abs.),

t = mean bulk temperature of fluid, (° F. abs.),

t_s = surface temperature, (° F. abs.),

t' = $t + (t_s - t)/4$ for Re below 2100, (° F. abs.),

= $t + (t_s - t)/2$ for Re above 2100, (° F. abs.),

u = local velocity of fluid, ft./sec.,

V = average velocity of fluid, ft./sec.,

v = specific volume of fluid, ft.^{3}/lb.,

X = roughness factor, dimensionless,

$$= \frac{\Delta p_{obs.}}{\Delta p_{theor.}}$$

x = height of conduit above arbitrary datum, ft.,

α = $4h/DGc$, ft.$^{-1}$

μ = viscosity of fluid at mean bulk temperature, centipoises,

μ_s = viscosity of fluid at surface temperature, centipoises.

References

1. Clapp, M. H. and Fitzsimons, O. S.M. thesis in Chemical Engineering. Massachusetts Institute of Technology. 1928.
2. Cope, W. F. Proc. Inst. Mech. Engrs. (London), 145 : 99. 1941.
3. Drew, T. B., Koo, E. C., and McAdams, W. H. Trans. Am. Inst. Chem. Engrs. 28 : 56. 1932.
4. Hagen, G. Ann. Physik, Poggendorf, 46 : 423. 1839.
5. Keevil, C. S. Sc.D. thesis in Chemical Engineering. Massachusetts Institute of Technology. 1930.
6. Keevil, C. S. and McAdams, W. H. Chem. & Met. Eng. 36 : 464. 1929.
7. Kemler, E. Trans. Am. Soc. Mech. Engrs. HYD-55 : 7. 1933.
8. Lee, A., Nelson, W. O., Cherry, V. H., and Boelter, L. M. K. Proc. Intern. Congr. Applied Mech. 5th Congr. Massachusetts Institute of Technology. 1938.
9. Martinelli, R. C., Southwell, C. J., Alves, G., Craig, H. L., and Weinberg, E. B. Trans. Am. Inst. Chem. Engrs. 38 : 493. 1942.
10. McAdams, W. H. Heat transmission. 1st ed. McGraw-Hill Book Company, Inc., New York. 1933.

11. POISEUILLE, J. L. M. Compt. rend. 15 : 1167. 1842; Mem. par divers savants. Acad. roy. sci. 9 : 433. 1846.
12. ROHONCZI, G. Eidgenöss. Materialprüf. u. Versuchsanstalt Ind., Bauw. u. Gewerbe, Zurich, Ber. No. 115. 1939.
13. SCHILLER, L. Forschungsarbeiten, 248 : 8. 1922; Z. angew. Math. Mech. 2 : 96. 1922.
14. SHERWOOD, T. K., KILEY, D. D., and MANGSEN, G. E. Ind. Eng. Chem. 24 : 273. 1932.
15. SIEDER, E. N. and TATE, G. E. Ind. Eng. Chem. 28 : 1429. 1936.
16. STODOLA, A. Steam and gas turbines, Vol. 1. *Translated by* Louis C. Loewenstein from 6th German ed. McGraw-Hill Book Company, Inc., New York. 1927.
17. WALKER, W. H., LEWIS, W. K., MCADAMS, W. H., and GILLILAND, E. R. Principles of chemical engineering. 3rd ed. McGraw-Hill Book Company, Inc., New York. 1937.
18. WHITE, J. B. S.M. thesis in Chemical Engineering. Massachusetts Institute of Technology. 1928.

THE DETERMINATION OF THE EFFICIENCY OF A HYDRAULIC TURBINE BY A CALORIMETRIC METHOD[1]

By John Katzman

Abstract

Western Electric bead type thermistors were used to determine the difference in temperature of the water between the headrace and tailrace of a hydraulic turbine at different loads on the turbine. From this temperature difference the maximum efficiency of the turbine was determined to be 92% and the unit flow of water in cubic feet per second was calculated.

Introduction

The calorimetric method for the determination of the efficiency of a hydraulic turbine was first developed in Europe (1), but only to a small extent. The temperature of water is increased by approximately $\frac{h}{778}$ ° F. when the water falls through a height of h feet. When this water passes through a hydraulic turbine at the lower level, the amount of energy taken from the water will show as a decrease in the temperature of the water; this decrease will depend upon the load on the turbine. The difference of the temperature of the water at the headrace and at the tailrace was obtained by means of thermistors.

This problem was brought to the attention of the author by the Shawinigan Water and Power Company. The measurements were made at the Shawinigan Water and Power Company powerhouse at Grand'Mère, Quebec, Canada.

Experimental

Two Western Electric bead type thermistors whose resistance at the ice point differed by only 0.6% were chosen from a group of eight. These thermistors were chosen because the measurements were made when the temperature of the water was 32° F. The thermistors were fixed by means of paraffin wax in brass tubes with small copper tips, Fig. 1. A small amount of mercury was placed at the bottom of the tip for better thermal contact. The tubes were fitted with $1\frac{1}{4}$ in. brass unions with which the unit was attached to the supporting pipes that held them in place in the water.

Each thermistor was connected as one arm of a Wheatstone bridge, Fig. 2. The other two arms were respectively, a 10,000 ohm Leeds & Northrup "unmounted resistor" and a similar one of 9500 ohms connected to a Leeds & Northrup decade box of 999.9 ohms. A galvanometer (sensitivity, 0.26 μv. per mm. at one meter) was used as a null point instrument. Six volts was impressed on the bridge. The galvanometer was mounted on a shock proof support.

[1] *Manuscript received August 24, 1948.*

Contribution from the Division of Physics, National Research Laboratories, Ottawa, Canada. Issued as N.R.C. No. 1851.

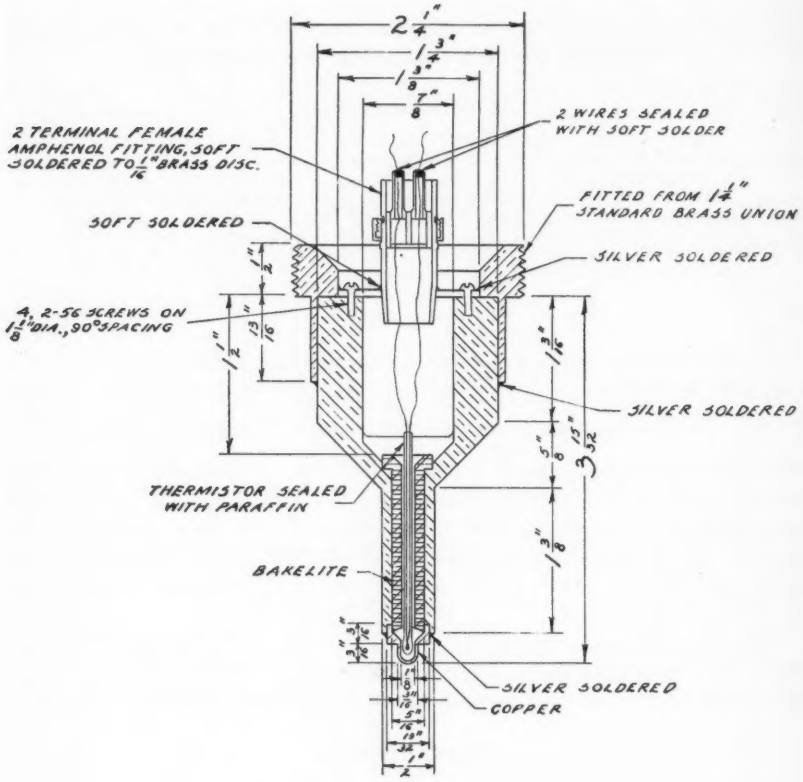

FIG. 1. *Thermistor housing.*

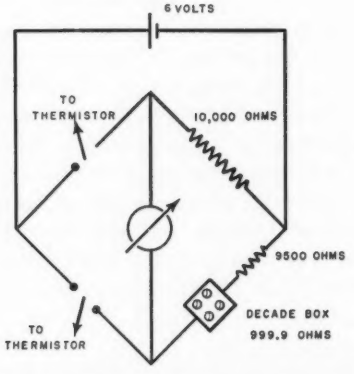

FIG. 2. *Wheatstone bridge arrangement.*

To calibrate the bridge the thermistors were placed in a vessel of two compartments, Fig. 3. Each compartment measured 2 × 2 × 2 ft. and was filled with 200 lb. of crushed ice that was intimately mixed with water. Both

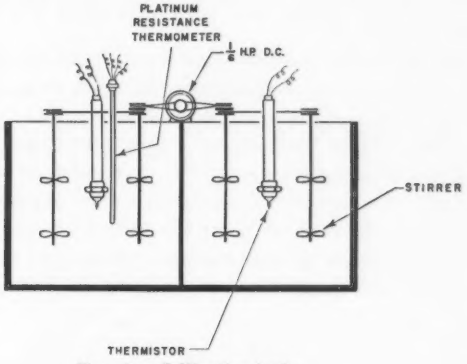

FIG. 3. *Calibration baths.*

thermistors were placed in one compartment and a bridge balance obtained. The thermistors were then placed separately in the ice baths and a platinum resistance thermometer was fixed beside one of the thermistors. Small quantities of sodium chloride were added to the ice–water mixture in which the resistance thermometer was placed. It was thus possible to obtain a bath whose temperature could be varied by small amounts. For each change in temperature by the one bath the bridge was balanced. The change in resistance necessary to balance the bridge was plotted against the change in temperature, Fig. 4.

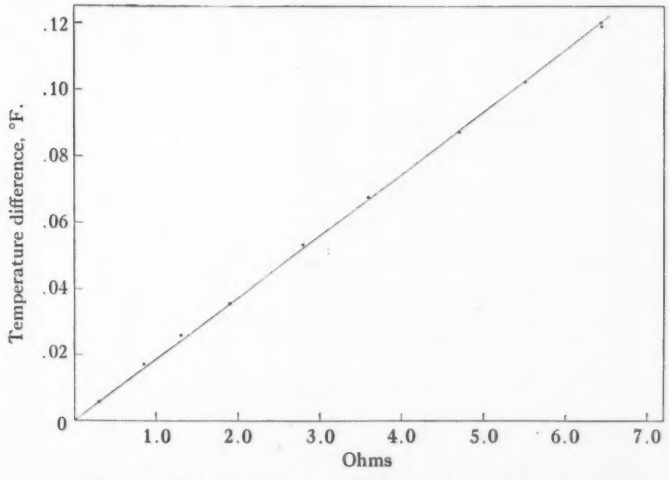

FIG. 4. *Calibration curve of the Wheatstone bridge arrangement.*

Tests

The No. 2 unit of the nine units at the powerhouse at Grand'Mère, Quebec, was chosen for test. All tests were made on Sundays because only then could the load on the turbine be varied at will and the unit could be put on independent hand control.

Both thermistors were lowered into the water of the headrace at the emergency gate opening and a balance on the bridge was obtained; this value was used as the zero. Then one thermistor was placed in position in the headrace and the other in the tailrace. The thermistor at the headrace was moved up and down for a distance of 20 ft. to determine whether the temperature of the water was uniform with depth. No change in temperature with depth was found. The same held for the tailrace. Temperature differences were measured for various gate openings, and at the same time readings of the turbine output and head of water were obtained from the control room.

Results

The results obtained are shown in Table I. Examination of the divided differences of the temperature difference indicated that, apart from random fluctuations, the relation of the temperature difference to the turbine output over the range studied could be adequately represented by a parabolic equation.

TABLE I

Temperature difference, °F.	Turbine output, megawatts	Gate opening, %	Operating head, ft.	Temperature difference, °F.	Turbine output, megawatts	Gate opening, %	Operating head, ft.
0.104	1.0	22.5	84.2	0.030	11.8	55.0	84.2
0.087	1.2	22.5	85.4	0.017	12.2	57.5	84.1
0.082	1.3	25.0	85.4	0.015	12.3	55.0	85.3
0.087	2.0	25.0	84.3	0.012	12.6	57.5	85.1
0.066	3.0	27.5	84.5	0.017	12.8	60.0	82.9
0.052	3.4	27.5	85.3	0.012	13.4	60.0	85.4
0.059	4.0	30.0	84.3	0.014	14.0	62.5	85.2
0.057	4.2	30.0	85.5	0.007	15.0	65.0	85.4
0.054	4.8	32.5	84.4	0.008	15.8	67.5	84.0
0.042	5.2	32.5	85.3	0.007	15.8	67.5	85.1
0.049	5.8	35.0	84.2	0.005	15.8	70.0	85.1
0.042	6.0	35.0	85.4	0.009	16.8	72.5	85.1
0.042	6.6	37.5	84.2	0.005	17.2	75.0	85.4
0.025	6.8	37.5	85.2	0.009	17.6	77.5	85.1
0.037	7.6	40.0	84.2	0.010	17.6	80.0	83.1
0.027	7.8	40.0	85.4	0.007	17.8	80.0	85.3
0.032	8.0	42.5	84.1	0.010	17.8	82.5	83.9
0.020	8.6	42.5	85.1	0.010	18.0	82.5	85.1
0.030	9.0	45.0	84.2	0.012	18.0	85.0	83.9
0.018	9.4	45.0	85.4	0.010	18.2	87.5	83.9
0.023	9.8	47.5	84.1	0.010	18.2	91.25	83.9
0.015	9.8	47.5	85.1	0.009	18.3	85.0	85.3
0.027	10.6	50.0	84.2	0.012	18.3	87.5	85.0
0.022	10.8	50.0	85.4	0.014	18.3	90.0	85.2
0.025	11.2	52.5	84.1	0.015	18.3	91.25	85.1
0.020	11.4	52.5	85.1	—	—	—	—

The parameters of such an equation were determined by the method of Least Squares by Mr. B. I. Wallace, Division of Biology, National Research Council of Canada. It was found that

$$t = 0.0999 - 0.0115x + 0.000362x^2, \tag{1}$$

where t is the temperature difference in degrees Fahrenheit and x is the turbine output in megawatts. The plot of this equation is shown in Fig. 5.

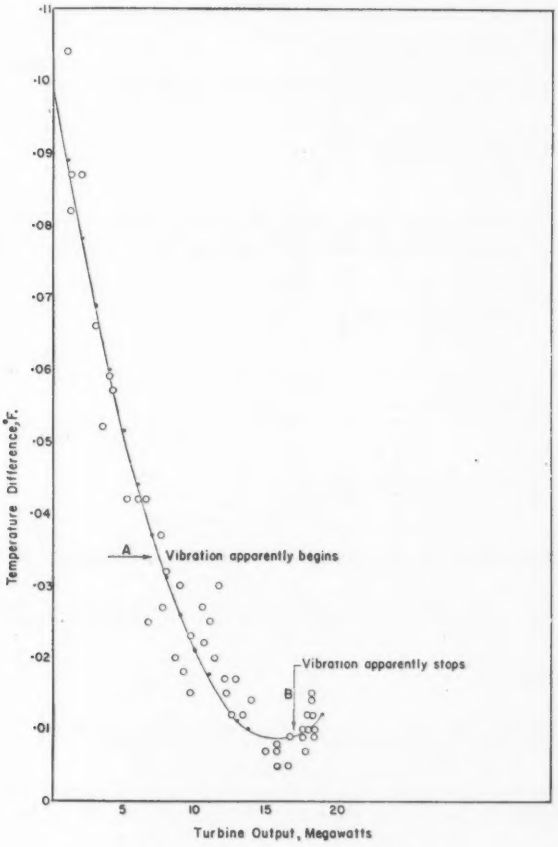

FIG. 5. *Turbine efficiency curve.*

The maximum efficiency is obtained when $\frac{dt}{dx} = 0$,

$$\frac{dt}{dx} = -0.0115 + 0.000752x$$

$$\therefore x \text{ max.} = 15{,}290 \text{ kw.}$$

that is, at a gate opening of 65%, Fig. 7, *B*. Substituting this value in Equation (1), $t = 0.0085°$ F., and hence the maximum turbine efficiency is 92%.

The flow of water through a turbine can be determined if the temperature difference, the height of water, and turbine output are known.

Let P = horsepower obtainable for a height of water, h ft.,

p = turbine output, horsepower,

f = flow of water, c.f.s.,

t = temperature difference, ° F. (measured).

Then $P = \dfrac{fh \times 62.4}{550} = \dfrac{fh}{8.8}$.

The temperature difference measured will be the temperature difference $\frac{h}{778}$ minus the loss in temperature difference caused by the turbine output.

$$\text{i.e., } t = \frac{h}{778}\left(1 - \frac{p}{P}\right).$$

$$\text{But } P = \frac{fh}{8.8},$$

$$\therefore f = \frac{p}{0.1136h - 88.4t} \tag{2}$$

If the turbine output is measured in horsepower, Equation (1) becomes

$$t = 0.0999 - (0.858 \times 10^{-5})\, p + (0.2015 \times 10^{-9})\, p^2. \tag{3}$$

From Equation (2)

$$t = \frac{1}{88.4}\left(0.1136h - \frac{p}{f}\right).$$

Substituting this value for t in Equation (3) and putting $h = 84.7$, we obtain,

$$\frac{1}{f} = \frac{0.792}{p} + 0.0007585 - (17.813 \times 10^{-9})\, p. \tag{4}$$

The plot of this equation is shown in Fig. 6, and the calculated values in Table II.

The most efficient flow is at 1900 c.f.s.

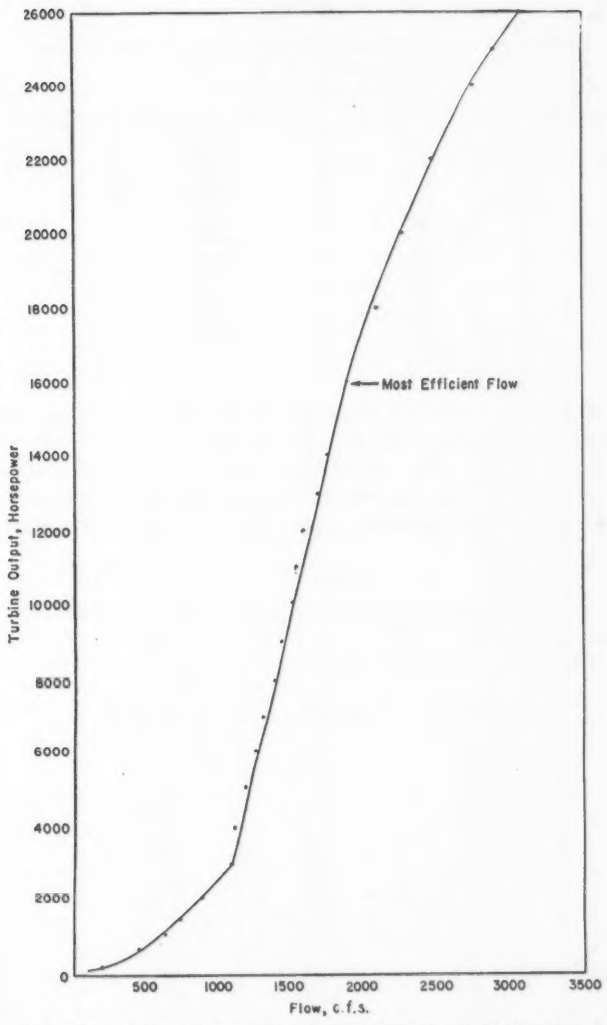

FIG. 6. *Flow of water through the turbine in cubic feet per second at various loads on the turbine.*

Three curves are shown in Fig. 7 that are of interest. Curve *A* is the plot of the gate opening against the temperature difference in degrees Fahrenheit, Curve *B* is of the gate opening against the turbine output in horsepower, and Curve *C* is of the gate opening against calculated flow in cubic feet per second. The variation in efficiency of the unit as determined by this method is shown by Curve *A*. The efficiency increases rapidly to a gate opening of about 50%, then not so rapidly to a maximum efficiency at a gate opening of 65%, and

TABLE II

CALCULATED UNIT DISCHARGE IN CUBIC FEET PER SECOND FOR DIFFERENT LOADS ON THE TURBINE

Turbine output, hp.	Unit discharge, c.f.s.	Turbine output, hp.	Unit discharge, c.f.s.
200	212	10000	1516
600	483	11000	1544
1000	652	12000	1604
1400	769	13000	1701
2000	894	14000	1768
3000	1104	16000	1912
4000	1129	18000	2100
5000	1207	20000	2263
6000	1277	22000	2483
7000	1339	24000	2747
8000	1399	26000	3079
9000	1457		

then drops off slowly. Curve *B* is the plot obtained from the figures supplied by the powerhouse operator and it indicates maximum efficiency at a gate opening of about 70%. The values represented by dots of Curve *C* were obtained from Equation (4), the crosses representing the values obtained from Equation (2) when the temperature and turbine output are averaged for each gate opening, Table III.

TABLE III

TEMPERATURE DIFFERENCE AND TURBINE OUTPUT AVERAGED FOR EACH SETTING OF THE GATE OPENING, FULL GATE = 100%; UNIT DISCHARGE OBTAINED FROM FIG. 8

Gate opening, %	Temperature difference, ° F.	Turbine output		Unit discharge, c.f.s.
		Megawatts	Horsepower	
22.5	0.096	1.1	1475	780
25.0	0.085	1.65	2211	950
27.5	0.059	3.2	4288	1175
30.0	0.058	4.1	5494	1250
32.5	0.048	5.0	6700	1325
35.0	0.046	5.9	7906	1400
37.5	0.034	6.7	8978	1460
40.0	0.032	7.7	10318	1550
42.5	0.026	8.3	11122	1 00
45.0	0.024	9.2	12328	1675
47.5	0.019	9.8	13132	1725
50.0	0.025	10.7	14418	1800
52.5	0.023	11.3	15142	1850
55.0	0.023	12.05	16147	1900
57.5	0.015	12.4	16616	1950
60.0	0.015	13.1	17554	2025
62.5	0.014	14.0	18760	2125
65.0	0.007	15.0	20100	2275
67.5	0.008	15.8	21172	2375
70.0	0.005	15.8	21172	2375
72.5	0.009	16.8	22512	2550
75.0	0.005	17.2	23048	2625
77.5	0.009	17.6	23584	2700
80.0	0.009	17.7	23718	2725
82.5	0.010	17.9	24016	2750
85.0	0.011	18.15	24321	2800
87.5	0.011	18.25	24455	2830
90.0	0.014	18.3	24522	2850

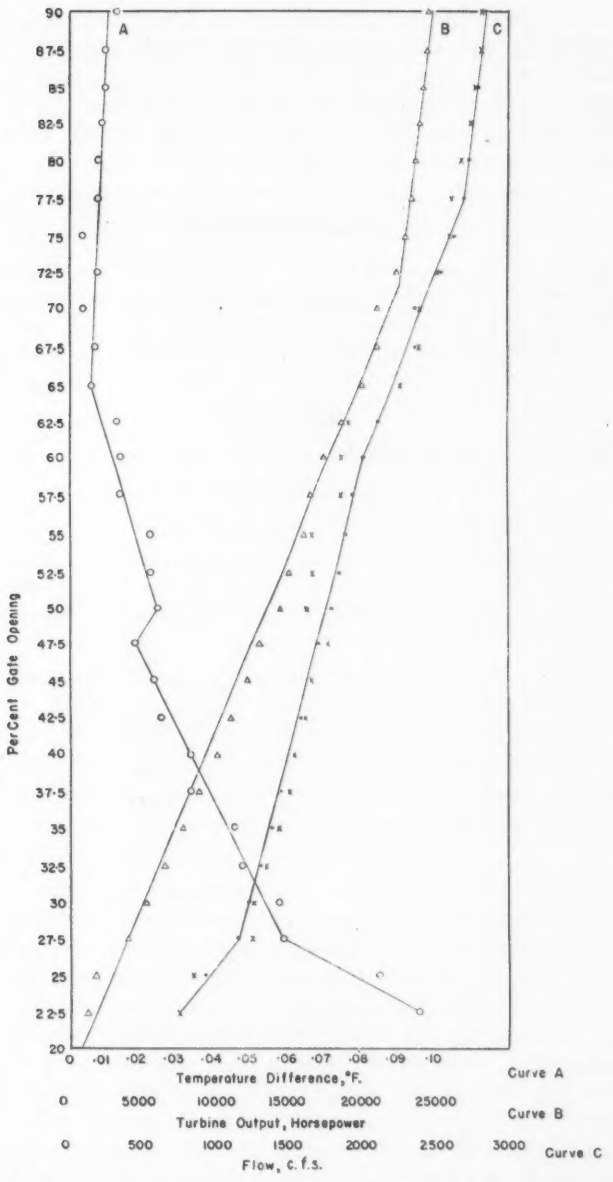

FIG. 7. *Effect of gate opening on the temperature difference between the headrace and the tailrace (Curve A), the turbine output (Curve B), the flow of water through the turbine (Curve C).*

It was noted that vibration of the power unit would begin at a gate opening of about 40%, increase to a maximum at about 55%, and then decrease until it could not be felt at about 70%. This vibration would cause fluctuations in the temperature of the water at the tailrace and is shown by the scatter of the values of Fig. 5 between the points marked *A* and *B*, and also by the crosses of Curve *C*, Fig. 7.

Acknowledgments

The author wishes to thank Mr. C. St. Jacques of the Physics Division, National Research Council of Canada, for the manner in which he assembled the apparatus and his assistance at the time of the tests, and Mr. W. R. McLeay, superintendent of the powerhouse for his keen co-operation.

Reference

1. UMPFENBACH, K. J. Z. Ver. deut. Ing. 81 : 1203. 1937.

CANADIAN AERIAL MAGNETIC SURVEYS (M.A.D.)[1]

By Ralph Bailey

Abstract

Tests concluded with an airborne magnetic detector measuring the earth's total field indicate a high degree of accuracy and speed for reconnaissance work over large areas. Cheapness of operation and freedom from small local anomalies make this a valuable tool for geophysical prospecting.

Introduction

For many years the measurement of magnetic anomalies in the terrestrial field has been a valuable method in geological studies and mineral location. To be able to map field variations rapidly by means of airborne equipment is an important advance in the application of geophysics to prospecting. This is now possible as a result of an intensive effort during the war to develop an airborne magnetic detector for submarine detection.

The purpose of this report is to describe the use of this instrument for studying magnetic contours over areas known to contain magnetic minerals, and the method by which these data may be presented so that they may be useful to those familiar with the interpretation of magnetic maps in relation to the geology of the area.

Many types of instruments depending on magnetic field variations were tried for detecting purposes during the war. Co-operation between the allied research laboratories was always possible and parallel development was carried out to meet specific requirements of the different armed services. Several types of magnetometers were made in the National Research Laboratories, Ottawa, and used in problems relating to harbor protection, automatic boat steering, and location of lost equipment.

Experience in this field indicated that an airborne type would have immense value in geophysical prospecting; consequently, immediately after the war, work was started to investigate the best way to use it for that purpose. The most advanced airborne type was that developed by the U.S. Naval Ordnance Laboratory. Though early experiments were carried out here with magnetometers designed in the National Research Laboratories, it was soon apparent that the applications of these instruments to geophysical prospecting would proceed most expeditiously by obtaining instruments already well developed. Accordingly, visits were made to Washington that resulted in the assistance and co-operation available there in putting this wartime development into practical use. Magnetic detectors were made available to the National

[1] *Manuscript received August 5, 1948.*

Contribution from the Division of Physics, National Research Laboratories, Ottawa, Canada. Issued as N.R.C. No. 1852.

Research Laboratories of Canada for government supported research that would further basic knowledge of geophysical and terrestrial magnetic problems.

The instruments used in the experiment described here were those developed by the Bell Telephone Laboratories under contract with the U.S. Naval Ordnance Laboratory and manufactured by the Western Electric Company for the Navy Bureau of Aeronautics. These instruments were obtained through the kind co-operation of U.S. Naval Ordnance Laboratory with whom friendly liaison had been maintained in various other magnetic problems during the recent war. It is our desire here to express thanks to the U.S. Navy, particularly the Bureau of Aeronautics and the Ordnance Laboratory, for making the Magnetic Airborne Detector (M.A.D.) equipment available to us. Thanks are also due the United States Geological Survey for their kindness in sending the M.A.D. equipped plane to Canada to demonstrate this new method of survey and for their help in introducing us to survey methods and map-making technique. Personal thanks are due Dr. L. H. Rumbaugh of the U.S. Naval Ordnance Laboratories, Commander J. W. Joyce of the U.S. Naval Bureau of Aeronautics, Mr. Homer Jensen, formerly of the U.S. Naval Ordnance Laboratories, and Mr. James R. Balsley, Jr., and his associates of the United States Geological Survey.

Parallel with the experiments described here the development of M.A.D. as a prospecting instrument was progressing much more rapidly in the United States. At the time of writing, hundreds of thousands of square miles of country have been covered, and more types of instruments are becoming available, so that their use in prospecting is already a commercial proposition.

The Instrument

The purpose of this instrument is to detect anomalies in the earth's magnetic field associated with the presence of oil or minerals. The sensitive part of the instrument consists of three magnetometer elements (of the second harmonic fluxgate type) mutually perpendicular to one another (2). Two of these elements, operating normal to the earth's field, control servo systems which maintain the third element in the earth's total field. The whole detecting mechanism is towed in a bomb-shaped housing sufficiently far from the aircraft to escape the effects of the magnetic field of the aircraft itself. The variations in the output of the element maintained in the direction of the total field are recorded on a simple recording milliammeter.

To follow the description refer to Fig. 8. Two gimbals whose axes of rotation are normal to each other are driven independently by two servo motors. They are maintained within three-quarters of a degree of the direction of null field and can be corrected with a maximum angular velocity of 20° per sec. The inner gimbal carries a Lucite cylinder containing the three separate magnetometer elements at right angles to each other. The middle element is used as a detector. The outside element perpendicular to

the axis of mounting is called the transverse element, while the other, mounted along the axis of rotation, is referred to as the axial coil. When the axial and transverse elements are in zero field the detector element is in total field. Any movement that destroys this orientation causes the axial and transverse elements to produce a signal proportional to the sine of the angular displacement, while the detector element (in total field) produces a change in signal of less magnitude since it varies as the cosine of the displacement from total field. The mechanism, therefore, operating to keep the detector element in total field, is activated by a signal that is large in comparison to the detector increment—the one that is used for measurement.

The detector element consists of a strip or cylinder of permalloy that is excited by a sinusoidal alternating voltage carried by a coil of wire around the strip of permalloy. In a steady magnetic field the current wave in the coil resulting from the sinusoidal exciting voltage becomes unsymmetrical and a prominent second harmonic appears. This harmonic is roughly a linear function of the steady field and hence it can be used for measurement. The second harmonic (2000 cycles) is separated from the exciting voltage (1000 cycles) by feeding it through a band pass filter of high quality, then to the amplifier, which serves to bring it to a usable level.

A 1000 cycle oscillator (V7 and V8, Figs. 5 and 6) set to $\pm$ 3 cycles provides exciting current through 1000 cycle filters to each of the three fluxgate elements. It also feeds a doubling circuit (V2) to produce 2000 cycles for the servo motor's power. A second oscillator (V1) provides an output of 2130 cycles ($\pm$ 5 cycles), which, when mixed in V6 with the 2000 cycles from the doubling circuit, provides 130 cycles for one phase of each of the two phase servo motors. The output from the detector element is applied to an amplifier (V1 and V4, Figs. 5 and 7) through a 2000 cycle filter. Since the sensitivity of the element is 35 μv. per gamma at the input to the amplifier there would be a signal of 2.1 v. on the grid of the first tube if the total field was 60,000 gammas. To eliminate the difficulty of handling a large output signal, a large portion of the average earth's field is balanced out by a direct current through the coil of the magnetometer element. In the present equipment all but 1500 gammas is so neutralized. The remaining average signal of 52.5 mv. is amplified in a conventional a-c. amplifier (V1 and V4) and rectified by a diode (V7), thus producing a d-c. potential (across R19).

As the recording instrument's sensitivity may be adjusted as high as 100 gammas for full scale, the amplified signal corresponding to 1500 gammas plus or minus the variations to be observed is still too high to feed directly to the recorder. The signal is therefore further controlled by imposing a d-c. neutralizing voltage (across R18) so that the output is zero for an arbitrary fixed steady field and produces plus and minus variations from this balance. These variations are fed to a d-c. amplifier (V9 and V10) after going through a sensitivity control circuit in the control box. The output (V10) is recorded directly.

The output from the axial fluxgate passes through a 2000 cycle filter to a second amplifier (V2 and V8, Figs. 5 and 7). It is then mixed with 2130 cycles (V10 and V5, Figs. 5 and 6) producing 130 cycles, which is amplified and fed to the second winding of the servo motor, which acts to bring this element into zero field. The output of the transverse fluxgate passes to a third amplifier and similarly to the second winding of the other servo. The 2000 cycle amplified outputs of the axial and transverse elements are also fed to separate rectifiers (V5 and V6, Figs. 5 and 7), yielding a d-c. component proportional to the square of the second harmonic signal voltage. These two d-c. components are then mixed and fed back through the control box and added to the detector output in an appropriate way to compensate for small and rapid misorientations.

The control box has been mentioned above in connection with the adjusting of the sensitivity and balance. Its functions are as follows. It attenuates the input to the d-c. amplifier so that the recorder scales will read 100, 200, 500, 1500, or 5000 gammas full scale. It effects the compensation required for the small and rapid misorientations referred to in the previous paragraph. It provides for the passing of d-c. increments through the detector coil in 50-, 500-, and 5000-gamma steps. This is accomplished by three parallel shunts across a $22\frac{1}{2}$ v. battery of large cell construction. Voltage is stabilized by rapid discharge to bring the battery to its plateau level. The control box load of 0.78 mill is then permanently applied. The battery remains useful for several months. The 50-gamma steps are obtained by the selection of proper fixed points across a voltage divider. The 500- and 5000-gamma steps are obtained by switching d-c. increments through the detector coil in such a manner that the impedance looking into the battery is constant.

The power pack is operated from 28 v. d-c. mains and consists of two dynamotors in parallel, feeding an electronically stabilized output circuit.

Method of Adjustment

Results with this instrument are obtained in the following manner. The instrument is first put in operation in a magnetically quiet location with no neutralizing d.c. in the coil of the detecting element. After the servo motors place the detector coil in total field, direct current is gradually increased in the detector until the total earth's field exceeds the neutralizing field by 1500 gammas, i.e., the instrument is undernulled by 1500 gammas. (This 1500 gammas is an arbitrary figure and was chosen since it is a suitable value for the type of anomalies encountered.) The recorder now reads zero for reasons shown above.

For calibration the instrument is set in operation and a set of Helmholtz coils is placed coaxially with the detector element so that known fields may be added to or subtracted from the earth's total field.

Values indicated on the recorder are therefore departures from average total field, and the term "profile," as used in this report, refers to the graphs of these variations.

The sensitivity of the instrument may be made to correspond to 100 gammas for full scale on the Esterline Angus recorder, or by various steps to 5000 gammas full scale.

The absolute value of the field, of course, is not known or recorded unless a specific procedure is adopted whereby the instrument is calibrated at a base station whose absolute value is known. For magnetic survey work this is not necessary, as only anomalies are measured. The compensating voltage may be maintained quite uniform and the gain of the amplifiers is reasonably stable so that the total field is probably indicated with a consistency of 1% from day to day. Variation over a short time can be read to a few gammas and drifts are very small when temperatures are steady.

Note:—Just before the work at the airport was terminated, the apparatus was operated continuously for a few days in an effort to observe diurnal changes. The detector was placed in a weatherproof box 200 ft. from the hangar while other equipment remained inside. Temperature has a considerable effect on the indicated field reading. However, since compensation is made for such changes in the Survey Procedure no further time has been given to the matter.

Survey Procedure

The area selected for the experimental survey lay some 25 miles west of Ottawa. The survey was conducted by flying half-mile grids at each of three elevations, 5000, 1000, and 500 ft. The method of survey was as follows. Half-mile grid lines (north–south) were drawn on one-mile-to-the-inch topographical maps. (Suitable aerial mosaics were not available.)

The crew of the Anson plane carrying the apparatus consisted of the pilot, navigator, magnetometer operator, and usually a fourth member who operated the winch, etc. The pilot was responsible for following the grid lines and maintaining constant altitude and speed. The navigator traced the plane's course on the topographical map and aided the pilot in his duty of following the grid lines by indicating land marks.

While flying the north–south grid, a note was made of the magnetically flat and the magnetically rough areas. This enabled the selection of an area suitable for flying an east–west base line to bring all north–south lines to a common denominator necessitated by diurnal and other magnetic changes and instrument drift.

A Sonne continuous strip camera (Fig. 3) was in operation during all flights. When passing over easily identifiable points, the navigator operated a foot pedal that linked the magnetic reading with that particular geographical position. This was accomplished by means of a photographic and electromagnetic system.

The recorder used was an Esterline Angus. While it was satisfactory in other respects, we found the chart rather narrow for the purpose. During flight, it is therefore necessary to observe the meter and maintain proper

placement of the pen by applying and recording known increments to the neutralizing circuit. This results in a discontinuous profile on the recorder tape The control box and linkages from it to the recorder (Fig. 4) so operate that increments in the neutralizing field and changes in sensitivity are printed on the tape.

By reference to the developed film, the flight lines are redrawn to coincide with the actual path of the plane. The geographical check numbers are also plotted on these flight lines from the film. The Esterline Angus tape with the magnetic record is then placed on the graph rectifier (Fig. 9). This is a machine with a system of levers and two movable tables to (*a*) convert the curvilinear record of the recorder tape to one with rectilinear co-ordinates, (*b*) expand or compress the horizontal scale so as to fit the desired map scale, (*c*) increase or decrease the vertical scale, and (*d*) fit the offset segments of the magnetic profile on the Esterline Angus tape into a continuous profile. The east–west base line profile values are then established where they geographically coincide with the north–south flight line profile values, and the comparison is noted. If there has been no terrestrial magnetic change, if there has been no instrumental drift, and if the geographical positioning is exact—then these values will be equal. If they are unequal it is necessary to adjust the reference line for each north–south profile to compensate for this difference. Flight lines flown over a period of hours, days, or months can therefore be tied together by a base line that can be flown in a few minutes, thus eliminating the possible errors due to drift, temperature, etc.

Suitable magnetic intensity values are next read from the north–south profiles (Fig. 10) and transferred to the flight lines (Fig. 11) obtained from the continuous strip film. The magnetic highs and lows are noted and magnetic contours drawn.

Three factors must be taken into account before magnetic values can be assigned a geographical position. They are distance of bird behind camera, lag due to recording, and perpendicularity of the camera.* Probably the simplest method for compensating for all three factors is to fly the base line first in an east–west direction then in a west–east direction. Peaks on these profiles should coincide when tied to geographical positions. If they do not coincide, a correction must be applied to all profiles, with due respect to direction of flight, and will be equal to half the distance between the baseline peaks.

Conclusions

The final contours are shown in Figs. 12, 13, and 14. All three levels were flown on half-mile grids. In the working up of the results this grid seemed quite suitable for the 5000 ft. level but was quite inadequate for the 500 ft. level.

The area was flown with the use of one-inch-to-the-mile topographical maps, which proved wholly unsuitable for wooded areas. In sparsely settled regions

* *The Sonne camera is gyro controlle d for roll but has no compensation for pitch.*

good aerial mosaics are essential if precision results are desired. The completed maps can be no more accurate than the positioning methods. It would be desirable if the present strip camera were stabilized for pitch as well as for roll, especially in rugged areas where the plane must climb rapidly on occasions.

A recording radio altimeter AN/APN1 was used, but it was not considered useful to attempt any correlation from the records when the 5000, 1000, and 500 ft. readings were already plotted. If something better than just general reconnaissance is required in magnetic mapping then an altimeter of much greater accuracy would be an improvement. In fact if sufficient precision were acquired it would be possible to construct topographical maps as well.

While the "winch, cable, and bird" has proved very satisfactory it adds to the need for greater precautionary measures. In this respect it is strongly recommended that (*a*) the amount of tow cable released from the winch be varied—say a foot or so per month of flying—so that the flexing occasioned at the point of suspension will not cause fatigue breakage (this flexing at the bird itself is taken up by a universal joint); (*b*) the whole apparatus be checked periodically; (*c*) a permanent, positive, semiautomatic device be installed for cable release in case of emergency; and (*d*) the whole system be subjected to periodic 500 lb. static load tests..

At the time of writing, the apparatus has been transferred to an inboard installation in a Canso aircraft. This eliminates the hazards associated with the towed bird system, which is used when only small planes are available.

This new method of prospecting places a powerful tool in the hands of the mining industry. The slow, laborious, and expensive method of point to point measurement can now be replaced by a cheaper one yielding a continuous magnetic profile at the rate of 120 m.p.h. Small surface anomalies that might otherwise mask or distort ground measurements are lessened, or completely wiped out, leaving only the general picture from which the over-all geological interpretation can be made. Drift and diurnal variations are minimized by the speed of operation and by the method of magnetic baseline corrections. There can be no doubt that the era of the dip needle for purposes of reconnaissance has disappeared, and will in future be reserved for necessary detailed surface work. The way is open for complete magnetic world coverage, which in time will aid in the better utilization of natural resources.

A modified instrument of this type will have extreme value in solving future navigational problems. Other instruments will be designed with a sensitivity as high as 0.1 gamma. Further, the principle will be applied in the construction of instruments for medical purposes, law enforcement, the location of lost objects, and laboratory and commercial use. The design of an absolute instrument for the recording and measurement of the earth's terrestrial field is in progress in this laboratory.

Acknowledgments

It is desired to express appreciation to Dr. R. W. Boyle for his continued aid and guidance, and to Dr. D. C. Rose for his constructive criticism.

Credit is due Mr. George Shaw, Geologist, Department of Mines and Resources, for his interest in this project since its beginning in 1946. To Mr. G. S. Levy of the Flight Research Section at Arnprior, we express our thanks for his co-operation in providing the necessary aerial facilities.

Fig. 1 appears through the courtesy of Mr. A. G. Roberts of the Capital Press Service in Ottawa.

References

1. EVE, A. S. and KEYS, D. A. Applied geophysics. Cambridge University Press, London. 1929.
2. FELCH, E. P., MEANS, W. J., SLONCZEWSKI, T., PARRATT, L. G., RUMBAUGH, L. H., and TICKNER, A. J. Trans. Am. Inst. Elec. Engrs. 66 : 641. 1947.
3. HAWKES, H. E. and BALSLEY, J. R. Magnetic exploration for iron ore in northern New York. United States Geological Survey, Washington, D.C. 1946.
4. RUMBAUGH, L. H. and JENSEN, H. U.S. Naval Ordnance Laboratory Report No. 937, Washington, D.C. 1945.
5. U.S. WAR DEPARTMENT, U.S. NAVY DEPARTMENT, and AIR COUNCIL OF THE UNITED KINGDOM. Handbook of maintenance instructions for AN/ASQ-3A equipment. Office of Publication Board, U.S. Department of Commerce, Washington, D.C. 1944.

PLATE I

FIG. 1. *M.A.D. in flight.*

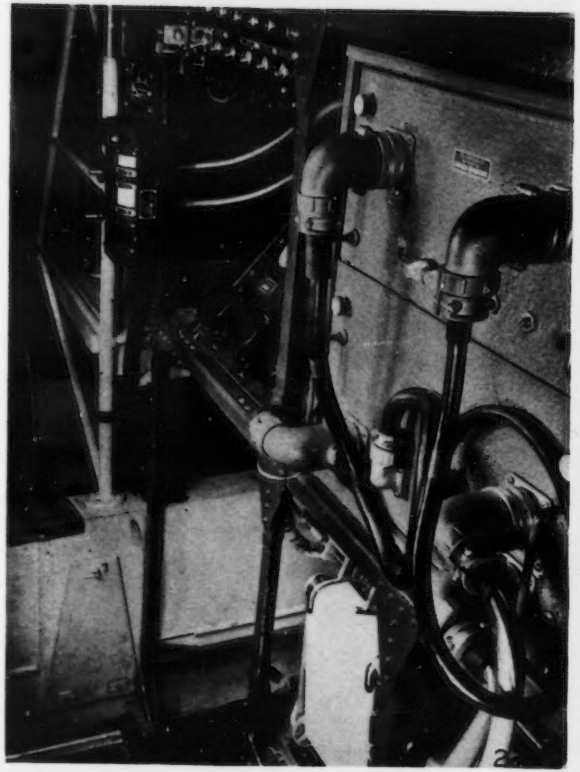

FIG. 2. *M.A.D. installation—Anson.*

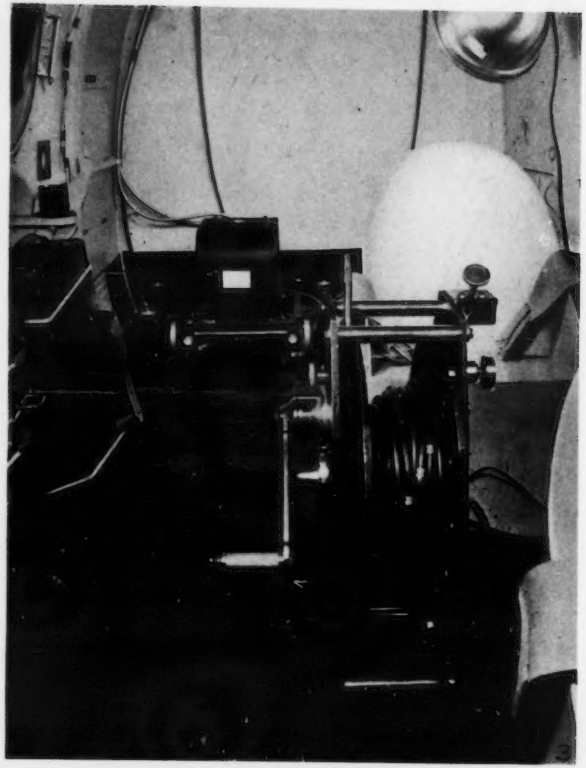

FIG. 3. *M.A.D. installation—Anson.*

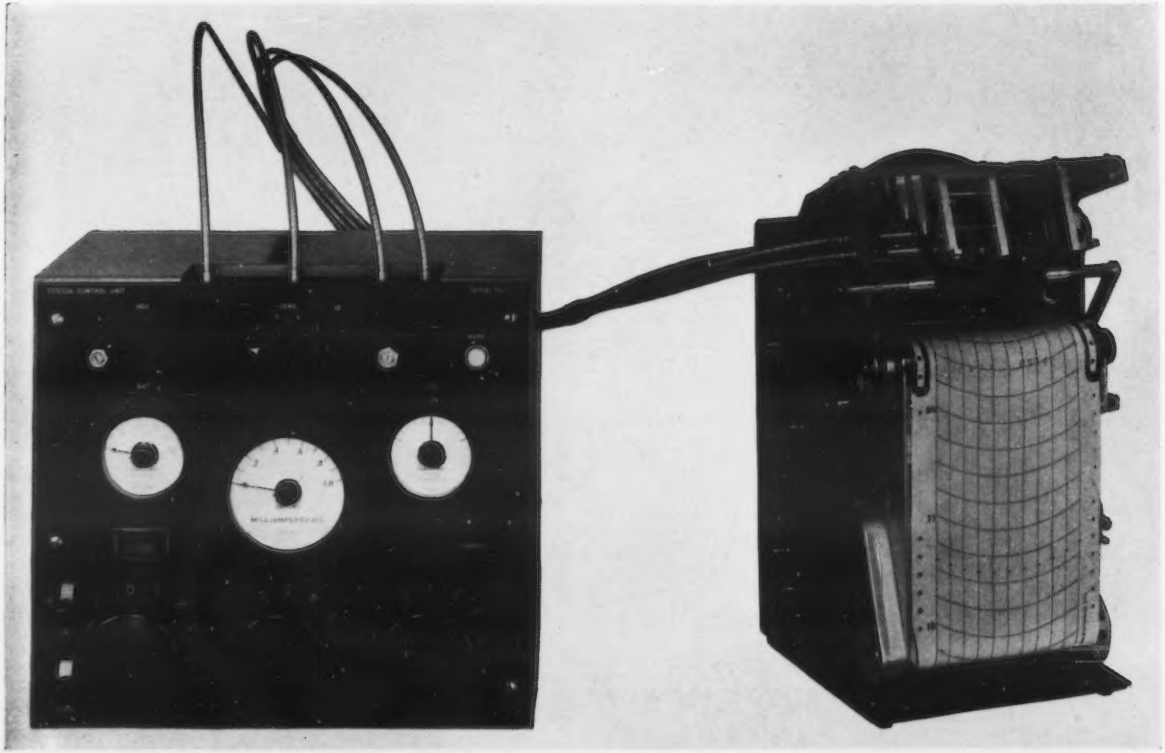

FIG. 4. *Control box and recorder.*

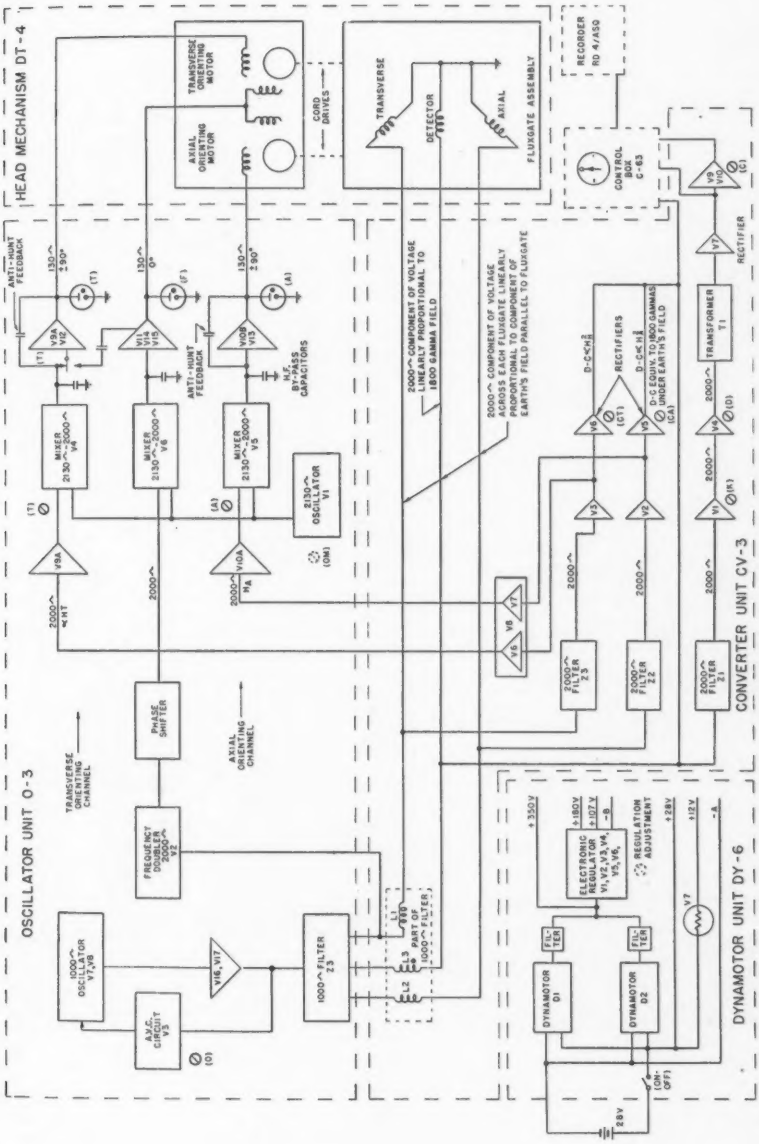

FIG. 5. *Block diagram. In this diagram, for "1800" read "1500".*

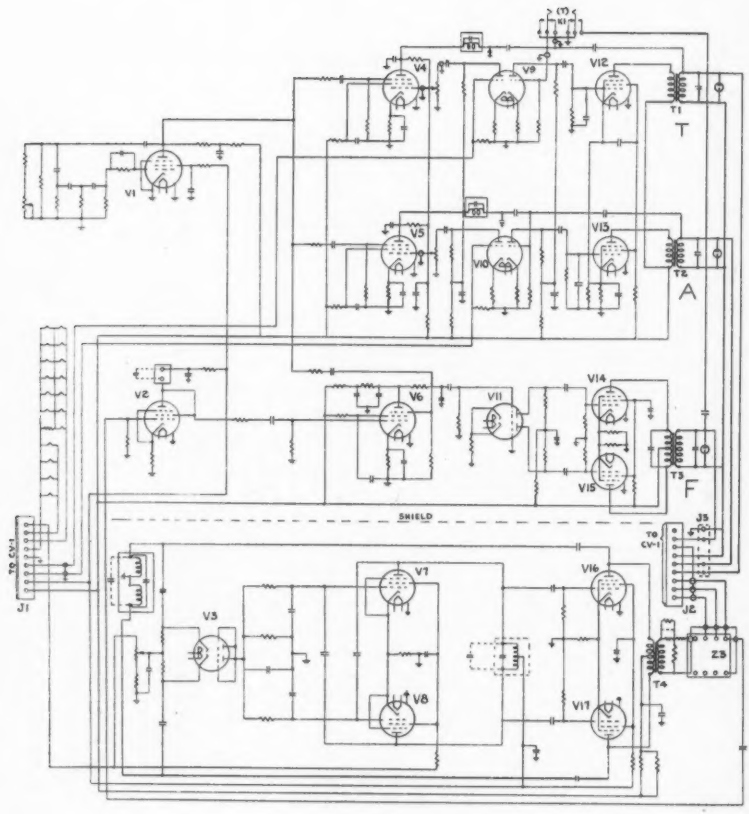

FIG. 6. *Oscillator.*

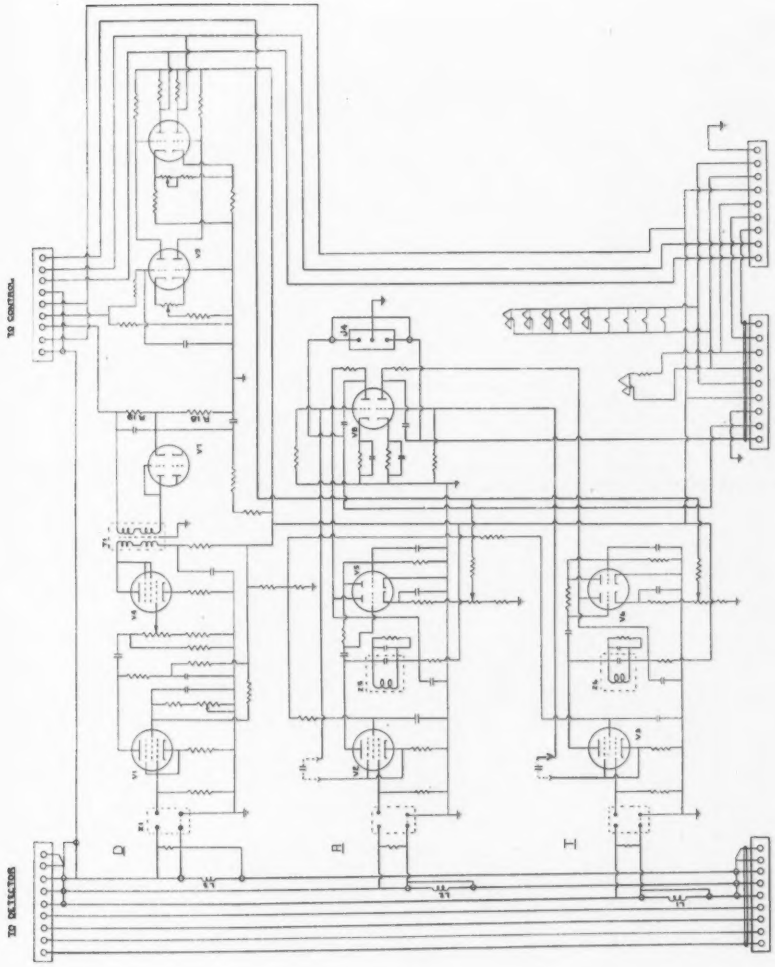

FIG. 7. *Converter unit.*

FIG. 8. *Magnetometer head, showing orienting gimbals and slip ring contacts. The three separate magnetometer elements are housed in the central Lucite cylinder.*

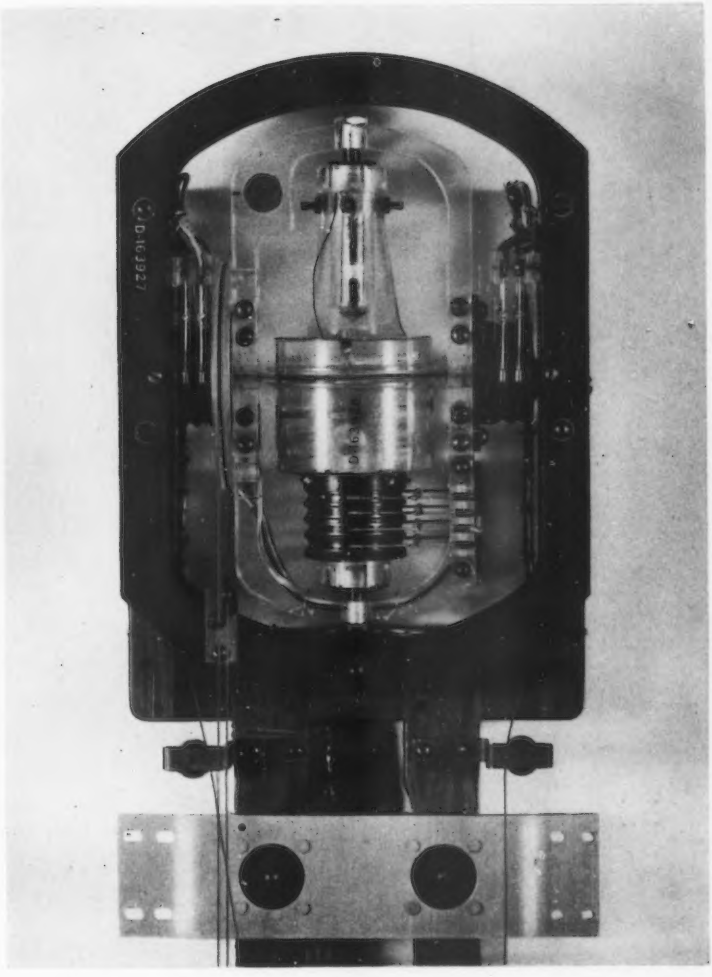

FIG. 8.

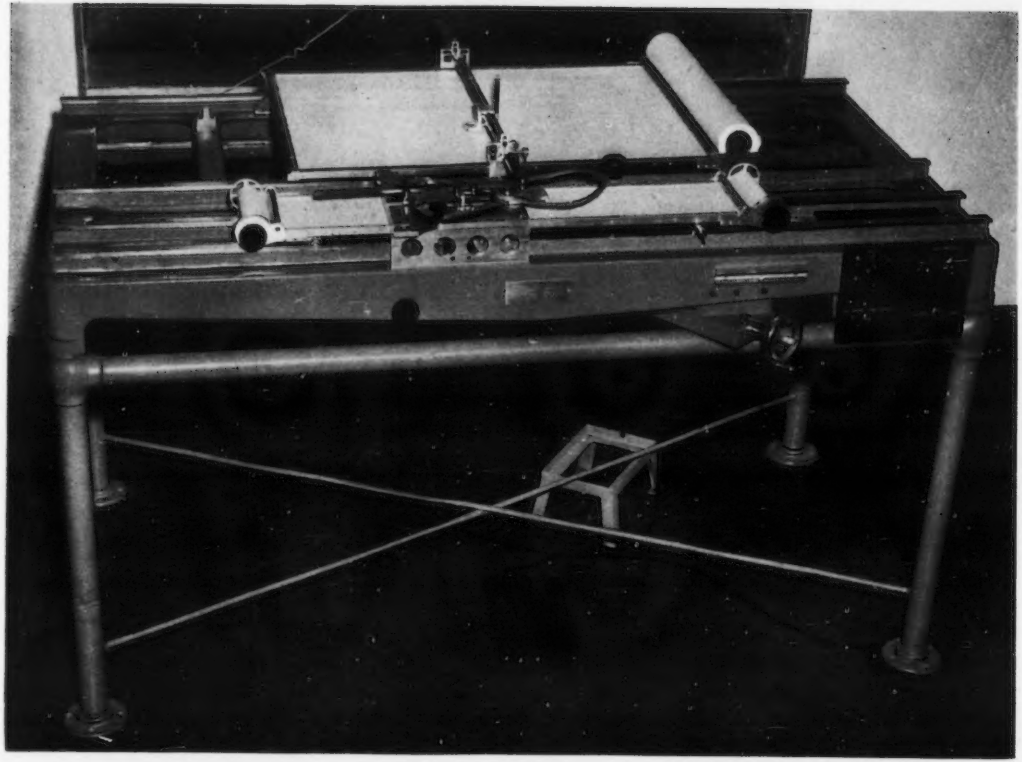

FIG. 9. *Graph rectifier.*

FIG. 10. *Magnetic profile. Line 17, 5000 ft. level, 500 γ sensitivity.*

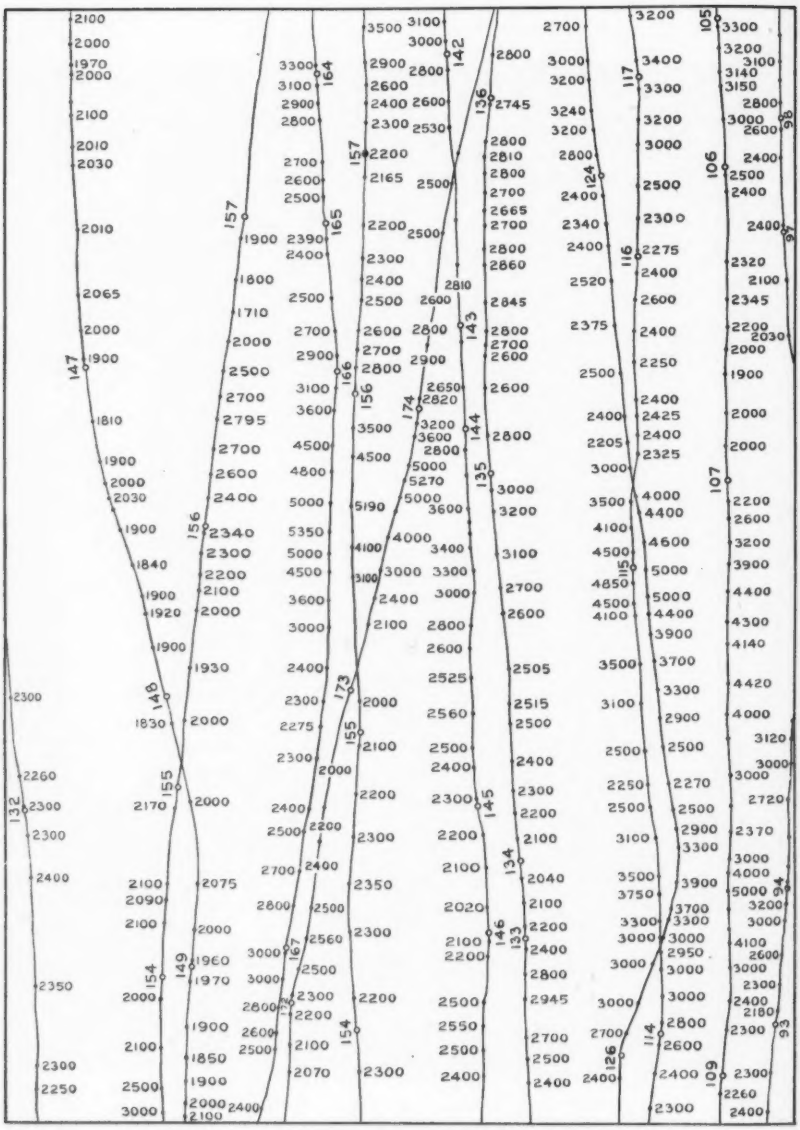

FIG. 11. *Flight lines with profile values (1000 ft. level).*

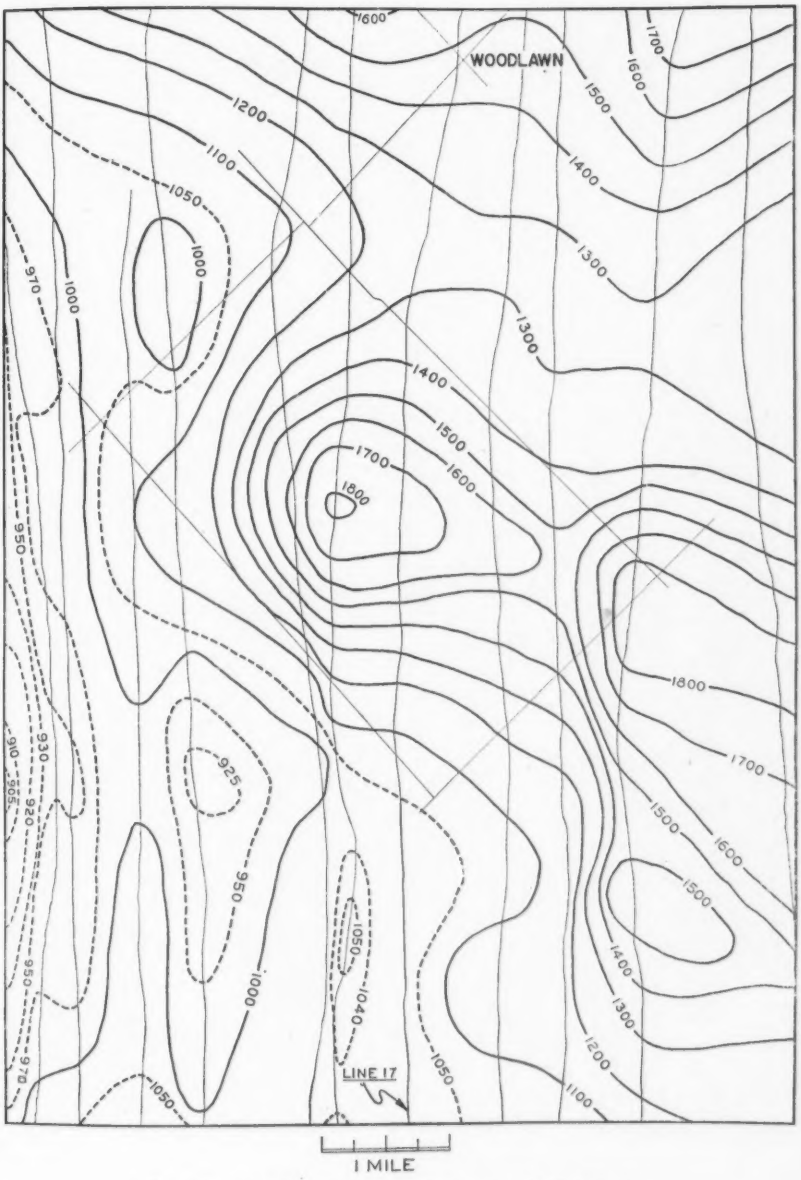

FIG. 12. *M.A.D. test survey. Carp area. 5000 ft. level.*

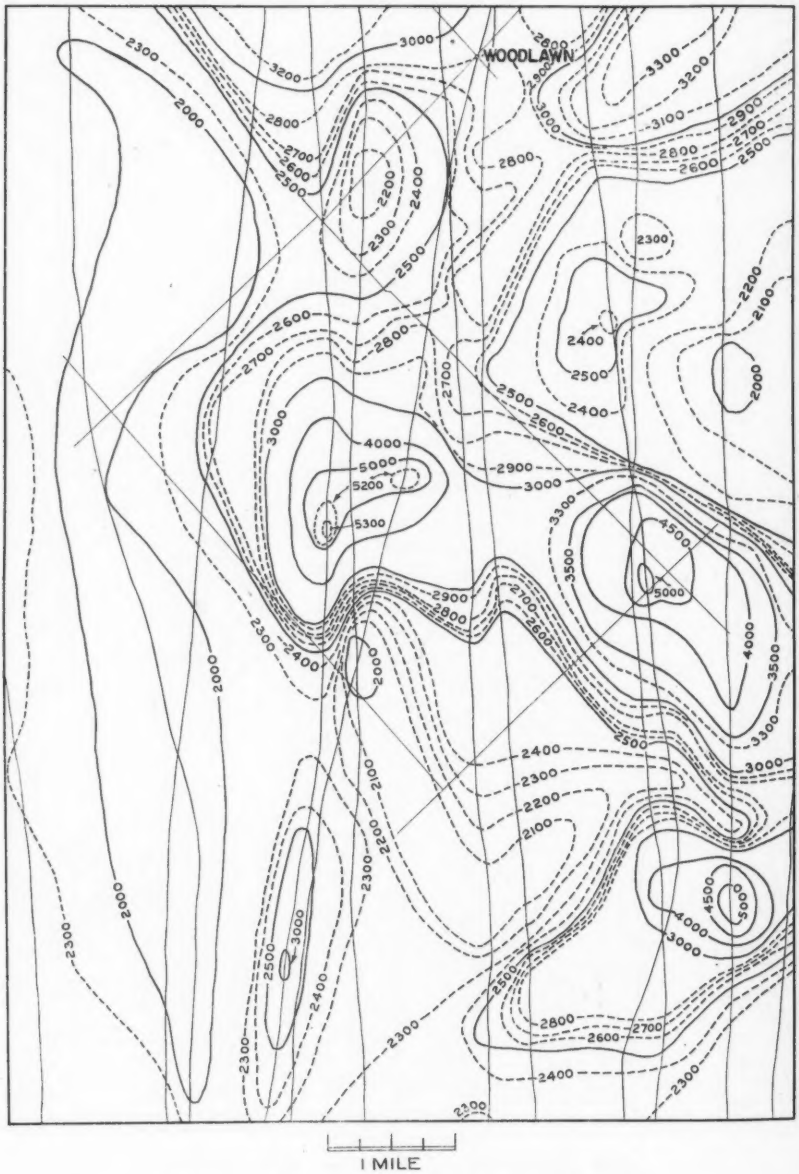

FIG. 13. *M.A.D. test survey. Carp area. 1000 ft. level.*

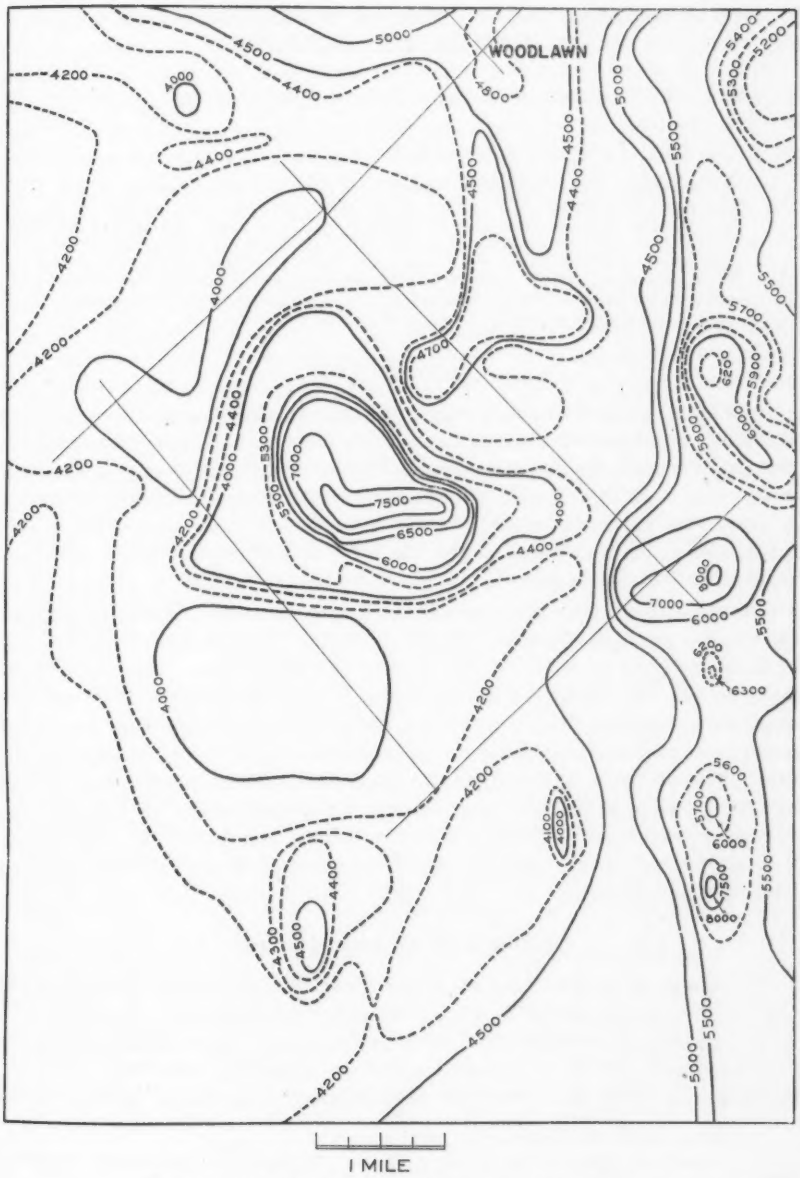

FIG. 14. *M.A.D. test survey. Carp area. 500 ft. level.*

THE FUNDAMENTAL ACTION OF INTENSIFYING SCREENS IN GAMMA RADIOGRAPHY[1]

E. L. HARRINGTON[2], H. E. JOHNS[3], A. P. WILES[4], AND C. GARRETT[4]

Abstract

The nature of the intensifying action of lead screens and Patterson screens has been investigated for gamma radiography. For the lead screens used it was found that nearly 52% of the blackening of the film is due to electrons ejected from the front screen and nearly 48% due to electrons ejected from the back screen. The blackening of the film due to the absorption by the film itself of the radiation is small. Similar results were obtained with Patterson screens except that about 10% of the effect of the screens is due to low energy radiation (light) which was stopped by 3 mgm. per cm.^{2} of aluminum.

Introduction

It is standard practice in gamma radiography to place the film between sheets of lead when making an exposure. The sheet of lead in front of the film usually has a thickness between 0.003 in. and 0.005 in., while the back screen may vary from 0.020 in. to 0.040 in. in thickness. With these screens in place, the exposure required for a photograph of a given casting is very much less than is required when the lead sheets are not used. For this reason the lead sheets are referred to as intensifying screens.

The cause of the intensification obtained with these screens was investigated by totally removing the effect of each screen in turn, and finally the effects of both of them, in order to find that of the film alone. The effect of the front screen was eliminated by separating the screen from the film and then applying a magnetic field in the region between the screen and the film strong enough to prevent any electrons ejected from the screen from reaching the film. For the back screen effect, an evacuated space was provided, instead of a back screen, sufficiently long to assure a negligible effect due to backward-moving electrons and radiation from the walls of the container. Finally, by a combination of both methods, the direct effect of the radiation on the film itself was determined.

Experimental Arrangement

The source of gamma rays used was a capsule containing 203.5 mgm. of radium, which was placed in a brass container having walls $\frac{1}{8}$ in. thick. To keep scattering to a minimum, a lead diaphragm, giving a total conical angle of 7° was used, and all interior surfaces of the apparatus were lined with light cardboard to stop scattered electrons without appreciable production of

[1] *Manuscript received September 2, 1948.*
Contribution from the Department of Physics, University of Saskatchewan, Saskatoon, Sask.

[2] *Professor and Head of the Department.*
[3] *Associate Professor of Physics.*
[4] *Graduate Student.*

X-rays. The source-to-film distance was kept constant at 9 in., and all exposures were made through $\frac{1}{2}$ in. of brass rather than steel since the apparatus had to be of nonmagnetic material. The radiographic properties of brass are close enough to those of steel to make the results applicable to either. The front lead screen was 0.003 in. thick, and the back screen 0.020 in. For the Patterson screens the industrial combination No. 245, with the thin screen in front, was used. Kodak No-Screen film was used throughout and developed in Kodalk X-Ray Developer, at 20° C., for five minutes, with agitation at the end of every minute. The film densities were read on a Marshall Transmission Densitometer.

To provide a constant check on the work, a control exposure was made and developed with each set of exposures. For this, a cardboard film holder, having a set of lead screens, or Patterson screens, the same as those used in the other parts of the experiment, was placed under a $\frac{1}{2}$ in. brass plate and given a constant exposure with a source to film distance of 9 in. The constant densities obtained for the control experiments indicated consistency of exposure, development, and film characteristics. As well as this, an unexposed strip of film was developed with each set of exposures to give the background density. The latter remained constant at 0.32.

Fig. 1 shows the exposure factor $\left(\frac{\text{mgm.} \times \text{min.}}{\text{in.}^2}\right)$ versus film density for the lead screens (Curve *A*), and the Patterson screens (Curve *B*) with Kodak No-Screen Film. These exposures were made with the film in firm contact with both the front and the back screen, the front screen being fastened to a

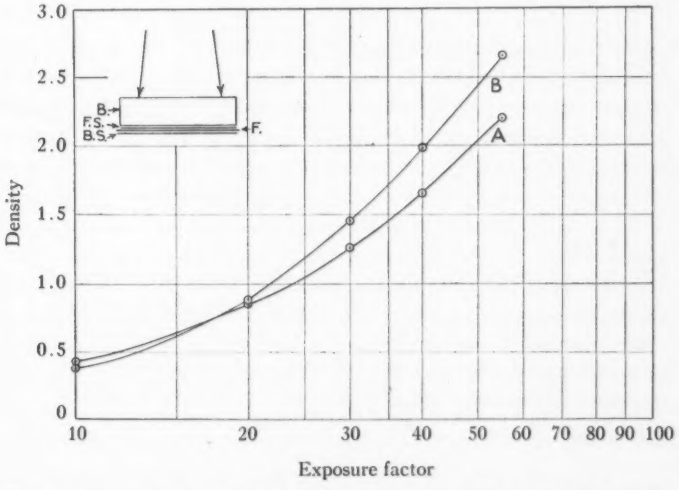

FIG. 1. *Density versus exposure factor for "No-Screen" film. Curve A was taken using a lead front screen 0.003 in. thick and a lead back screen 0.020 in. thick. Curve B was taken using Patterson Industrial Combination No. 245. The film was exposed through $\frac{1}{2}$ in. of brass. (B—brass, F.S.—front screen, F—film, B.S.—back screen.)*

brass plate ½ in. in thickness. In the following experiments, an exposure factor of 55 was used with the lead screens, and 45 with the Patterson screens. These exposure factors give a density of 2.21 in each case (see Fig. 1.)

Part I

Lead Screens

(*a*) *The Effect of the Front Screen*

Consider a magnetic field applied parallel to the front screen and perpendicular to the incident beam of gamma rays, as in Fig. 2. All ejected electrons will move in circular paths in the magnetic field, the curvatures of the paths

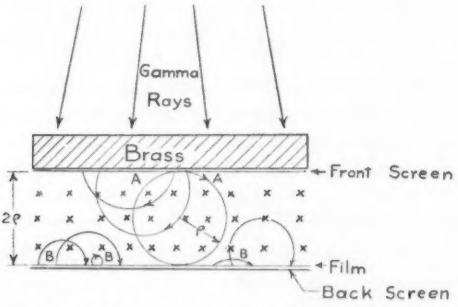

FIG. 2. *The schematic arrangement of the apparatus used for determining the effect of the front screen.*

being dependent on the energy of the electrons and on the strength of the magnetic field, and their excursions from the front screen on the direction of ejection from the screen into the field. Those that are ejected tangentially to the front screen towards the right (path *A*, Fig. 2) will be the hardest to prevent from reaching the film Electrons that follow a path having a radius of curvature greater than ρ and that are ejected tangentially (path *A*) will strike the film. 2ρ is the distance between the film and the screen and had the value 2.35 cm. in the apparatus used. It follows then that electrons with energies corresponding to values less than $B\rho$ (where *B* is the flux density) would all be prevented from reaching the film regardless of their directions of emission. Some electrons (see *B*, Fig. 2) will be ejected in a backward direction from the film itself, and these will be curved back into the film by the magnetic field and produce some darkening.

Fig. 3 shows the experimental arrangement used to determine the effect of the front screen. *N* and *S* are the poles of an electromagnet capable of giving a field of 5400 gauss across a gap of 3 cm. The film holder consisted of an air-tight metal box, which could be evacuated to cut down the scattering from the air in the box. The front screen was fastened to the ½ in. brass top

of the box, while the film and back screen were supported by a series of spacers. These spacers made it possible to vary the separation d between the front screen and the film from 1.50 cm. to 6.50 cm. in a series of five steps.

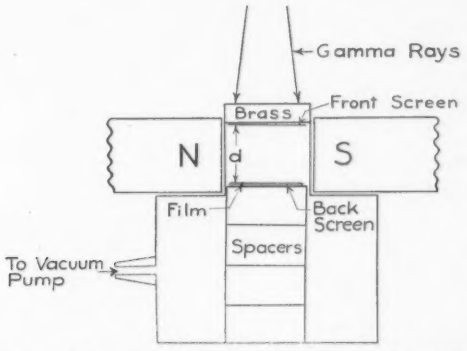

FIG. 3. *Diagram of the apparatus used to determine the effect of the front screen.*

Some of the exposures made to determine the effect of the front lead screen are listed in Table I. Only the average values of the densities obtained are

TABLE I

SUMMARY OF RESULTS OF THE DETERMINATION OF THE EFFECT OF THE LEAD FRONT SCREEN

Separation between front screen and the film, d cm.	Magnetic field, gauss	$B\rho$, gauss-cm.	Average density
0.00	0	0	2.21
2.35	0	0	1.21
2.35	1500	1760	1.05
2.35	2790	3280	0.93
2.35	4240	4980	0.89
2.35	5385	6325	0.89

given. The individual measurements agreed to within about 5%. These results appear graphically in Fig. 4.

It is seen from Table I that for zero magnetic field, a change in the distance between the front screen and the film from 0 cm. to 2.35 cm. causes a decrease in density from 2.21 to 1.21. A considerable decrease is to be expected as the distance d is increased. Also it will be seen from Fig. 4 that the density is constant for $B\rho$ equal to or greater than 4980 gauss-cm.

To correct the density at maximum magnetic field to zero centimeters of separation, a series of exposures was made with separations between the front screen and the film of 1.50, 2.35, 3.70, 5.00, and 6.50 cm. using the apparatus shown in Fig. 3. For all these exposures, the maximum field of 5385 gauss was

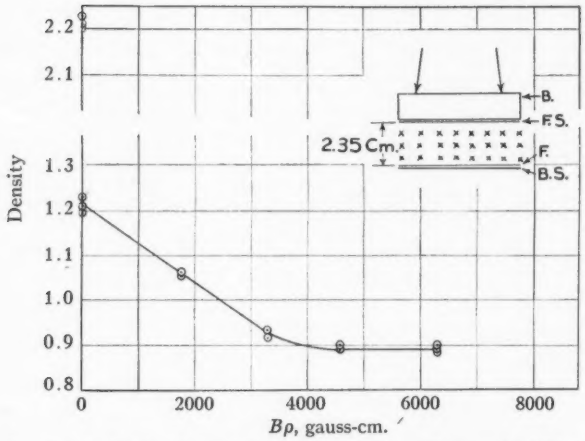

FIG. 4. *Graph showing the variation of film density with magnetic field when the electrons ejected from the front lead screen are curved back by the application of the magnetic field shown.*

applied in the region between the front screen and the film. The result of this series of exposures is shown in Fig. 5, in which density is plotted against

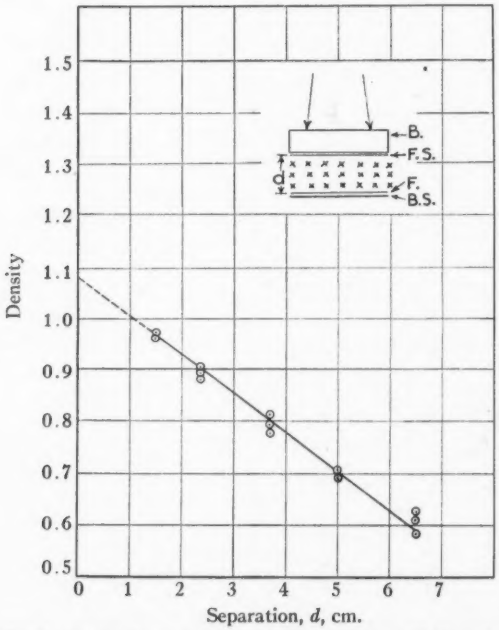

FIG. 5. *Graph showing the variation of the film density with the separation d between the front lead screen and the film when all the electrons ejected from the front lead screen are prevented from reaching the film by the magnetic field.*

the separation between the front screen and the film. For all the points plotted the magnetic field of 5385 gauss was sufficient to ensure the return to it of all the electrons emitted by the front screen in the forward direction. That is, these points correspond to points beyond the bend in the curve shown in Fig. 4. From Fig. 5, it is seen by extrapolation that for zero separation the density would be 1.08. This means that removing the effect of the front screen decreases the density from 2.21 to 1.08, a reduction of 51.2%.

From that portion of the curve in Fig. 4 where the density is constant it is possible to determine the maximum energy of the electrons emitted from the front screen owing to the action of the incident gamma rays. The value of $B\rho$ where the density becomes constant is 4980 gauss-cm., which corresponds to an electron energy of 1.07 Mev. for an electron ejected tangentially or 2.5 Mev. for an electron projected normally. The maximum energy of the incident gamma ray from radium is 2.2 Mev., which can eject from lead a photoelectron of energy 2.1 Mev. The probability of the photoelectron's being ejected in the forward direction is considerably greater than at an angle of 90°. When one considers that the 2.2 Mev. component of the gamma rays from radium is very small, we see why the bend of the curve in Fig. 4 appears in the region indicated.

(b) The Effect of the Back Screen

It was impossible to use a magnetic method to determine the back screen effect owing to the fact that there are a great many more electrons ejected from the film in the forward direction than in the backward direction. These would be curved back into the film by the magnetic field, and cause a very great increase in the density of the film. In a trial experiment the density obtained with 0 field was 1.42 and when the maximum field of 5385 gauss was applied the density rose to 1.62. For this reason, it was decided to remove the effect of the back screen by the use of distance only. The apparatus represented in Fig. 6 was used. It included a bell jar, 7 in. in diameter and 16 in. high, sealed onto a ½ in. brass plate. The front screen was fastened to the brass plate and the film held in firm contact with it. The bell jar was evacuated for all exposures, with all other conditions the same as for the front screen determination.

Exposures were made also with the back screen in contact with the film to serve as a check, and densities of 2.21 were obtained. This value is in agreement with Table I and Fig. 1 for an exposure factor of 55. Then the back screen was removed entirely, leaving only the film and the front screen, and several additional exposures were made. These gave densities that averaged 1.13. This means that the removal of the back screen reduced the density from 2.21 to 1.13, a reduction of 49.0%.

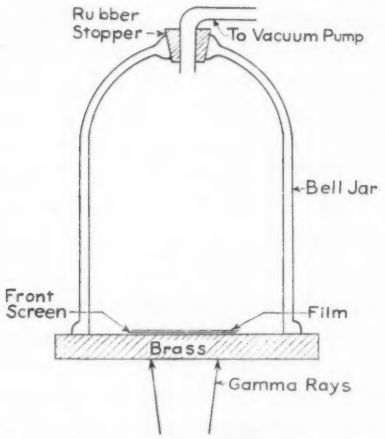

FIG. 6. *Diagram of the apparatus used to determine the effect of the back screen.*

(*c*) *The Effect of the Film Alone*

To determine the effect of the film alone, a combination of the two methods was employed. Fig. 7 shows the apparatus employed; it made use of an

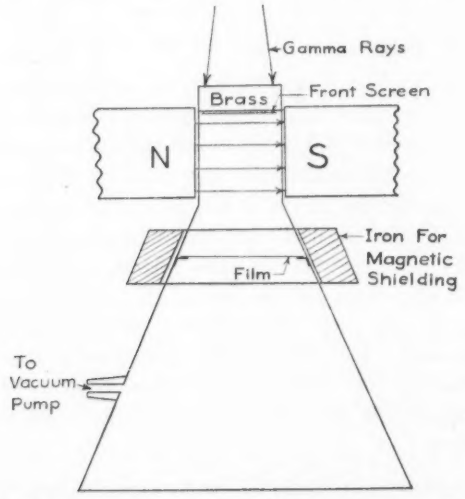

FIG. 7. *Diagram of the apparatus used for the determination of the effect of the film alone.*

air-tight box 13¼ in. high having a brass top ½ in. thick to which the front screen was attached. The film was supported 3¾ in. below the front screen, and a magnetic field of 5385 gauss was applied in the region indicated. A heavy iron bar was placed around the box in the region of the film to act as a magnetic shield and thus to provide a region of zero field at the position of

the film. This is necessary to prevent electrons ejected from the film from curving back into it and thus causing an increase in density. The bottom of the box was 9 in. below the film, and no back screen was used. The box was evacuated for all exposures.

Several exposures were made with the same conditions as in the other parts of the experiment described above. These gave an average density of 0.08 when, as in all cases, the background of 0.32 was subtracted. When the effects of both the front and back screen are removed, the density falls from 2.21 to 0.08; this indicates that the percentage effect of the film alone is 3.6%.

Part II

Patterson X-Ray Intensifying Screens, Industrial Combination No. 245

(a) Front Screen

The effect of the front screen was determined in the same manner as for the lead front screen but with the addition of one further step. This consisted of taking an additional series of exposures, varying the magnetic field as before, but having the front screen covered with a thin sheet of aluminum foil (3.05 mgm. per cm.^{2} This thickness of foil would not absorb any appreciable number of the electrons from the front screen yet would absorb the light emitted by these screens when they are irradiated with gamma rays. Fig. 8 shows the results of both these series of exposures, Curve *A* with the front screen alone, and Curve *B* with the front screen covered with aluminum foil.

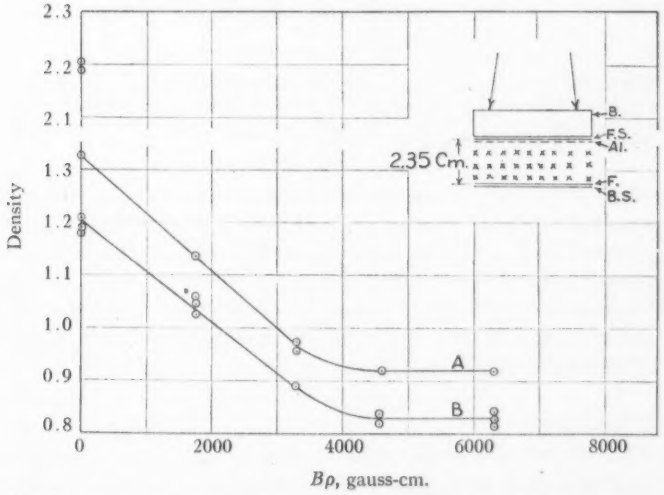

FIG. 8. *Graph showing the variation of film density with magnetic field when the electrons ejected from the front Patterson screen are curved back by the application of the magnetic field shown. For Graph B the Patterson front screen was covered by aluminum foil 3.05 mgm. per cm.^{2} thick. For Curve A no aluminum was used.*

Fig. 9 shows the result of varying the spacing between the front screen and film, and is analogous to Fig. 5 for the lead screens. From this graph it is seen that a density of 1.05 would be obtained at 0 cm. separation if all the

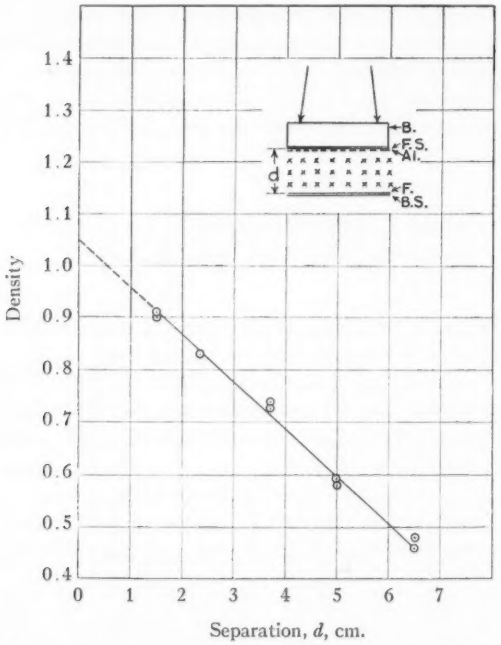

FIG. 9. *Graph showing the variation of the film density with the separation d between the front Patterson screen and the film when all the electrons ejected from the front screen are prevented from reaching the film by the magnetic field, and radiation from the front screen is filtered by 3.05 mgm. per cm.² of aluminum.*

electrons from the front screen were prevented from reaching the film and if radiation from the front screen that can be absorbed by 3.05 mgm. per cm.² of aluminum were stopped. This corresponds to a reduction in density of 1.15 and gives a Patterson front screen effect of 52.3%. From the displacement of the two curves in Fig. 8, it is seen that the light energy that can be stopped by 3.05 mgm. per cm.² of aluminum makes up 9.8% of the total effect of the Patterson front screen.

(b) Patterson Back Screen

The effect of the Patterson back screen was determined in exactly the same way as for the lead back screen. Exposures with both front and back screens present gave a density of 2.20, and, when the back screen was removed and a vacuum chamber employed, the density fell to 1.15. This means a reduction in density of 1.05, and gives a Patterson back screen effect of 47.8%.

(*c*) *The Film Alone*

The effect of the film alone was determined also for the Patterson screens in order to obtain a check on the work. The determination was made in exactly the same manner as when using the lead screens except in this case the front screen was covered with aluminum foil. The density obtained using an exposure factor of 45 was 0.075; this gave an effect of 3.4% for the film alone.

To determine whether bombardment of the lead screen by gamma radiation produces any appreciable amount of radiation in the visible or in the ultraviolet regions, two further exposures were made with the lead screens. The first one was made with a separation of 2.35 cm. between the front screen and the film with a field of 5385 gauss and the second similarly but with 3.05 mgm. per cm.^{2} of aluminum in contact with the lead front screen. These two exposures gave the same density; this indicated that if any radiation was produced in the lead front screen, it was penetrating enough to pass through 3.05 mgm. per cm.^{2} of aluminum.

Discussion of Errors

The gross percentage error for the experimental work was about 4%, which is made up of several factors. The source-to-film distance could be reproduced to $\pm$ 1/16 in., and the exposure times (21.9 min. for the lead screens, 18 min. for the Patterson screens) could be reproduced to $\pm$ 3 sec.

The processing of the exposed film was under very close control, as shown by the fact that the density of the control exposure and the unexposed background strip never varied more than $\pm$ 0.02.

Scattered radiation would increase the film density in all cases over that due to any direct radiation and to the electrons themselves. However, with the 7° collimator used in all parts of the experiment, and with all inner surfaces of the chamber lined with cardboard and the chamber evacuated, the scattered radiation was certainly reduced to a low value.

In the front screen determination the film was situated in a strong magnetic field so that any electrons that were ejected backward from the film were curved back into it and caused an increase in density. This effect certainly contributes some error but it should be small since comparatively few electrons are ejected backward. In the arrangement used in determining the effect of the film alone, the larger size of the apparatus made it possible to provide magnetic shielding for the region of the film, and thereby largely prevented an increase in density due to any curving-back effect.

Since the film had to be removed from the front screen by a finite distance for the front screen and the film alone effects, an indeterminate error was introduced. In the case of the front screen effect, while it was possible to extrapolate the curves of Figs. 5 and 9 to a 0 cm. separation, no proof could be obtained, owing to the lack of a sufficiently powerful magnetic field, that the curve continued as was assumed.

A further error is introduced by calculating the percentage effects as though the density versus exposure factor curves were linear, whereas they are slightly curved in the region used.

Discussion and Summary of Results

Table II gives a summary of the effects of the front and of the back screens, and of the film alone, for both lead screens and Patterson screens. The fact that the three effects add up to more than 100% in itself indicates the magnitude of the joint errors involved.

TABLE II

SUMMARY OF ALL THE RESULTS FOR LEAD SCREENS AND PATTERSON SCREENS

	Lead screens	Patterson screens
Exposure factor used	55	45
Maximum density	2.21	2.20
Front screen effect:		
(*a*) Due to electrons, %	51.2	42.5
(*b*) Due to light energy, %	0.0	9.8
(*c*) Total effect, %	51.2	52.3
Back screen effect, %	49.0	47.8
Film alone effect, %	3.6	3.4
Total	103.8	103.5

No check on the percentage of the Patterson back screens effect due to light energy could be obtained. However, it seems a safe assumption to say that it is of the same order of magnitude as that for the front screen.

The effects reported here were obtained for only one thickness of lead screens and one type of Patterson screen, and for one thickness of brass. It is probable that if these factors were changed the same general type of results would be obtained.

It is obvious from this table that the use of some form of intensifying screen is imperative in gamma radiography. That the effect of the film alone should be so small is understandable when it is realized that the only way in which gamma rays can cause darkening is by the ejection of electrons, and only those electrons having paths largely within the emulsion will produce any appreciable effect. Since the absorption by the film of gamma rays is small, comparatively few electrons are available for darkening. It is doubtful whether this fact has been fully appreciated by film manufacturers or users. The absorption of the gamma rays by the film could be increased if materials of high atomic number were incorporated in the emulsion. The fact that most of the darkening comes from the effects of the front and back screen is indicative of the care that should be taken in the choice of these screens.

The practical aspects of the choice of these screens from the point of view of the sensitivity obtainable and the intensification that can be secured has been discussed by some of the authors in another publication (1). It will suffice to state here that the screens should be maintained in firm contact with the film so that the electrons ejected from the screen will affect the film at their point of origin, rather than at a considerable distance, to avoid loss of sharpness. In the second place the screens should be clean. If a small section of the screen is covered with some foreign material, the latter will absorb the electrons from the screen and will produce only a smaller number of electrons owing to its own absorption of the gamma rays. This will result in a light spot on the film.

Acknowledgments

The authors wish to thank the National Research Council of Canada for their financial assistance in supporting this work, and especially Dr. W. A. Morrison of the Radiology Section of the National Research Council for his part in initiating this research. The authors are indebted to Mr. A. H. Cox of the instrument shop in the Department of Physics of the University of Saskatchewan for his technical assistance.

Reference

1. JOHNS, H. E. and GARRETT, C. Can. J. Research, A, 26 : 292-305. 1948.

ON THE EXTENDED USE OF KLEINLOGEL'S RAHMENFORMELN[1]

By I. F. Morrison[2]

Abstract

This paper contains but a single idea. Its purpose is to show how, by the use of Kleinlogel's Rahmenformeln, the number of simultaneous linear equations that occur in the analysis of indeterminate structures can be reduced materially by using a primary structure, itself made up of indeterminate parts, provided the bending moment diagrams can be drawn for them. These are obtained from the Rahmenformeln. In order to recall to the reader's mind the well known moment-area method a brief summary of that process is included. A practical numerical example of the analysis of a frame indeterminate to the seventh degree is worked out in detail. Two arrangements of the indeterminate components are chosen in the illustrative example. The final bending moment diagram is shown for a simple loading case and the influence line for the bending moment at one point is discussed briefly.

Introduction

During the recent war the Eighth Edition of Professor Kleinlogel's well known Rahmenformeln was reprinted in the United States by the authority of the Alien Property Custodian. It was published by Frederick Ungar Publishing Co. in 1943, supplemented with a crib in English—published separately—for the benefit of those not familiar with the German language.

This remarkable book contains diagrams and formulae for simple frames of various shapes, support conditions, and loadings. One hundred and fourteen frames are listed with 1643 diagrams accompanied by numerous formulae. The diagrams show the moment-curves for each case of loading; the formulae give the algebraic expressions for the moments, shears, and reactions. The index of contents is an odd one consisting, as it does, of a series of simple illustrations showing the shape and support conditions of each frame with the numbers of the pages on which the moment-curves and formulae pertaining to it will be found. A very brief introduction contains all the necessary information concerning notation, rules for signs, and other pertinent information. However, one does not need to be able to read this part to make use of the tables, which are quite obvious as to meaning. Besides, the English translation now available obviates this difficulty.

At first sight, one might think that this useful handbook would be limited in its application to only those cases contained in it. This is, however, a false conclusion for, although it is not so indicated in the introduction, the simple frames can be used as units with which to build up multiple frame structures of unlimited extent. By such synthesis, the use and value of the book becomes considerably extended and it is the purpose of this paper to

[1] *Manuscript received July 6, 1948.*

Contribution from the Department of Civil Engineering, University of Alberta, Edmonton, Alberta.

[2] *Professor of Applied Mechanics, University of Alberta.*

present a method by which the analysis of multiple frame structures may be carried out in a simple and direct manner based on the information contained in it.

This method, namely, the moment-area method, consists in dissociating the multiple frame into units that can be found in the text and in using these units as the elements of a primary structure. The elements themselves are statically indeterminate, but, since the analysis for them is already at hand in the text, no difficulty by way of preliminary analysis is present and the synthesis is carried out with these statically indeterminate units instead of the statically determinate units usually used for that purpose. The amount of effort required to analyze a highly indeterminate structure is enormously reduced and for that reason the analysis of multiple structural frames, which might appear as formidable, is brought within quite reasonable range.

The Moment-area Method

The purpose of this section is to recall to the mind of the reader the moment-area method.

In order to demonstrate this most useful, perhaps, of all methods of structural analysis, a simple algebraic example will be given. Consider a rigid frame as shown in Fig. 1 with which the reader will be undoubtedly quite familiar.

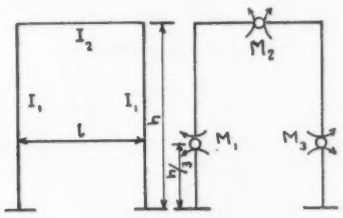

FIGS. 1 and 2.

This structure is indeterminate to the third degree, i.e., three unknown, or redundant, reactions in addition to the three reactions of plane statics are present, and, therefore, in addition to the three equations of equilibrium of plane statics, three additional equations in terms of the three redundants must be established. These form a system of independent, simultaneous, linear equations that must eventually be solved. The moment-area method is one that sets up these equations; it does not offer a method of solution of them. When they are few in number the solution of them can be easily and quickly accomplished.

The first step in the process is to render the indeterminate structure determinate by the insertion of suitable cuts and hinges. In the present case, this is shown in Fig. 2, in which three hinges have been inserted. The structure is now statically determinate and stable. This is called the "primary structure".

From the equations of virtual-work, the set of simultaneous equations involving the redundants M_1, M_2, and M_3, the unknown moments at the selected points of the indeterminate structure, are readily established. These may be written in condensed form as

$$\Sigma a_{ij}M_j = c_i \qquad i \text{ 1 to 3}$$

$$a_{ij} = a_{ji} \qquad j \text{ 1 to 3}$$

The c_i are the loading terms. It is easily shown that the a_{ij} are given by the "work equation" owing to a self-stressed condition. The most important

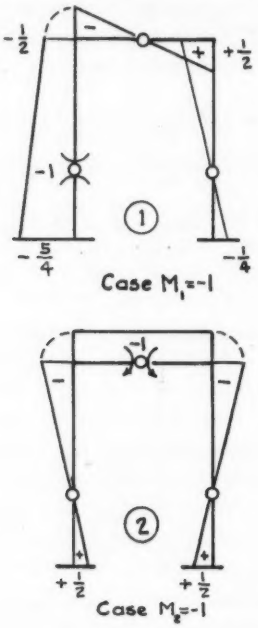

FIG. 3.

term in the complete work equation and the only one usually retained, but not necessarily so, in analysis of this sort is

$$a_{ij} = \Sigma \int_0^l \frac{M_i M_j ds}{EI}.$$

In this equation, the M_i and the M_j are the bending moments in each member due to a self-stressed condition imposed by placing successively at each hinge a couple, -1. The EI is the product of the modulus of elasticity by the moment of inertia of the cross section for each member. Since E is often constant and occurs on both sides of the equation, it will be assumed to

disappear from the following equations. The integration is taken over the length of each member and the summation sign indicates that the sum of these integrations must be taken.

This process requires three bending moment diagrams, two of which are shown in Figs. 3, (1), and 3, (2), respectively. The third is like 3, (1) except reversed. The areas so displayed on the diagrams are called moment-areas and the method takes its name from this fact.

The simple integrations for many cases have been worked out and are given in a table in Müller-Breslau's *Die Graphische Statik der Baukonstruktionen*, Band II, 2 abt. page 56. Many combinations of moment-areas are included in this table but here only one will be given which is all that is necessary for the present purpose.

Fig. 4 indicates the case referred to and shows two trapezoidal moment-areas that are to be multiplied and integrated from 0 to l. The factor $\frac{1}{EI}$

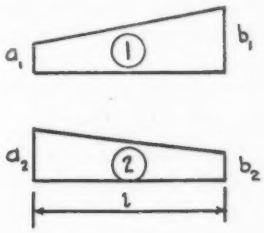

FIG. 4.

will be considered constant for the member and, therefore, omitted in the integration. Then

$$\frac{1}{EI}\int_0^l M_1 M_2 ds = \frac{l}{6EI}\left[a_1(2a_2 + b_2) + b_1(a_2 + 2b_2)\right].$$

The moment-areas 1 and 2 may be said to be "paired" by this process. The matrix a_{ij}, so to speak, represents the structure in mathematical form and might be called the "structure". It depends, however, on the choice of the primary structure. Owing to the assumptions of Hooke's law and elasticity of the members of the structure, the matrix is of necessity always symmetric.

Returning to the analysis, we have now to work out the six constants a_{ij} by pairing the moment-areas for the frame.

As a sample calculation, take a_{12}.

Starting with the left leg of the frame,

$$\int_0^l M_1 M_2 ds = -\frac{h}{6} \cdot \frac{3}{2} = -\frac{h}{4},$$

and proceeding around the frame, one finds

$$a_{12} = -\left(\frac{h}{4I_2} + 0 + \frac{h}{4I_2}\right) = -\frac{h}{2I_2}.$$

In the same way, all the other coefficients may be set down, practically by inspection. Thus, we have:

$$a_{11} = \frac{7}{8}\frac{h}{I_2} + \frac{1}{12}\frac{l}{I_1} \qquad a_{22} = +\frac{l}{I_1} \qquad a_{33} = \frac{7}{8}\frac{h}{I_2} + \frac{1}{12}\frac{l}{I_1}$$

$$a_{12} = -\frac{h}{2I_2} \qquad a_{23} = -\frac{h}{2I_2} \qquad a_{31} = -\left(\frac{1}{8}\frac{h}{I_2} + \frac{1}{12}\frac{l}{I_1}\right).$$

It is customary to indicate the ratio of the moment of inertia of a member to its length by a single letter, called the "stiffness factor." Here, however, we shall put $k = \frac{I_1}{I_2} \cdot \frac{h}{l}$, which is in concordance with Kleinlogel's formulae.

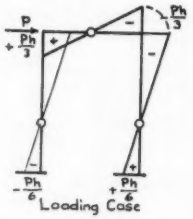

FIG. 5.

The loading terms are determined also from the moment-area of the primary structure, due to any specified loading on it, paired with each of the three self-stressed moment-areas. If, for example, the loading as shown in Fig. 5 be chosen, then

$$C_1 = -\frac{Ph}{12} \cdot \frac{h}{I_2} - \frac{Ph}{12} \cdot \frac{l}{I_1}$$

$$C_2 = +\frac{Ph}{6} \cdot \frac{h}{I_2}$$

$$C_3 = +\frac{Ph}{12} \cdot \frac{h}{I_2} + \frac{Ph}{12} \cdot \frac{l}{I_1}$$

The equations then become, in matrix form,

$$\begin{bmatrix} \frac{7}{8}k + \frac{1}{12}, & -\frac{k}{2}, & -\frac{1}{8}k - \frac{1}{12} \\ -\frac{k}{2}, & 1, & -\frac{k}{2} \\ -\frac{1}{8}k - \frac{1}{12}, & -\frac{k}{2}, & \frac{7}{8}k + \frac{1}{12} \end{bmatrix} \cdot \begin{bmatrix} M_1 \\ M_2 \\ M_3 \end{bmatrix} = \begin{bmatrix} -\frac{Ph}{12}(k+1) \\ +\frac{Ph}{6}k \\ +\frac{Ph}{12}(k+1) \end{bmatrix}$$

This completes the demonstration, for there is no point in solving these algebraic equations. The object has been merely to show how they are set up by means of the moment-area method. Of course, it is much more expedient to work directly with the numerical values.

Solution of the Equations

The main difficulty that arises in any method of analytical analysis of a highly indeterminate structure is in the solution of the large set of simultaneous equations that arise in the process. This becomes very tedious and great care is required in checking the solution as it progresses. For this reason any method by which the number of equations can be reduced offers a material advantage.

There are a number of methods that have been developed by which the number of simultaneous equations can be reduced. The present paper presents such a method. It is based, however, on the assumption that the moment-area diagrams for a number of simple, though statically indeterminate, frames are readily at hand as mentioned in the introduction. Kleinlogel's Rahmenformeln provides this information.

The Use of Kleinlogel's Rahmenformeln

We now turn to the use of Kleinlogel's diagrams. In the preceding moment-area method, the primary structure was chosen as statically determinate solely because it was easy to construct the bending moment diagrams for such a structure. In the Rahmenformeln, however, we have access to literally hundreds of cases of simple, indeterminate frames. Instead, then, of rendering the statically indeterminate structure determinate, to obtain a tractable primary structure, we may adopt a primary structure made up of frames the moment-areas of which are already known and therefore also easily handled.

This method of dissociating the structure into a primary structure, itself composed of indeterminate parts, reduces very materially the number of simultaneous equations to be solved, as will be seen in the following examples.

Numerical Examples

In order to illustrate the advantage so gained by this process, it is proposed to analyze the relatively simple structure shown in Fig. 6, *a*. First, the primary structure is decided upon. This may be done in several ways. In this case, the choice is shown in Fig. 6, *b*. The original structure is indeterminate to the seventh degree. By inserting two hinges as shown, the primary structure is indeterminate to the fourth degree.* In selecting the primary structure care must be exercised to select only such an arrangement of hinges or cuts as will leave the elements of the primary structure such that the moment-area diagram is already known. It should be noted that the shorten-

* *The left-hand hinge is on a horizontal shelf, so to speak, and removes two constraints. The right-hand hinge removes only one constraint.*

ing of the posts is assumed to be neglected as usual and, as a consequence, there will be no vertical displacement of the hinges. The solution is approximate in this respect.

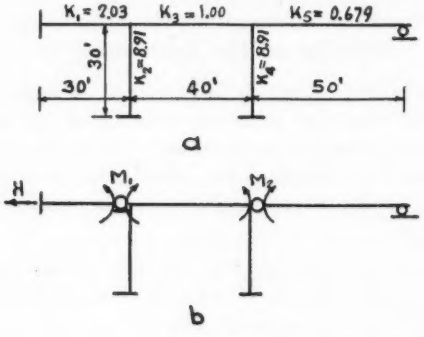

FIG. 6.

The values of k shown in Fig. 6, *a*, have been obtained by first selecting one value of the stiffness factor as a unit value and then finding the ratios of it to the respective stiffness factors of the remaining members. In the present case the girder of the center span was so chosen that $k_3 = \frac{I_3}{l_3} = 1$. Each pairing of the moment-areas is multiplied by the corresponding k-value for the member.

Since the structure is indeterminate to the seventh degree we would, if the primary structure were rendered determinate as in the usual procedure, have to determine $\frac{n(n+1)}{2} = 28$ independent coefficients, and $n = 7$ loading terms; in itself a formidable task. Then seven simultaneous linear equations would have to be solved; this is time consuming, to say the least.

By using the primary structure as composed of elements, themselves indeterminate, the number of equations to be solved has been reduced to three and the number of coefficients to six, thus effecting a very large saving of effort.

In any case, to determine the number of redundants, let n be the degree of indeterminateness of the structure and N the sum of the degrees of indeterminateness of the components of the primary structure, then the number of redundants, say R, is

$$R = n - N.$$

In the present case, the left-hand girder is indeterminate to the first degree*, the middle frame to the third degree, and the right-hand girder to the zero degree. Thus,

$$R = 7 - 4 = 3,$$

* *Note that the right-hand end of it is on a roller supported by the post.*

which is the number of redundants selected and shown in Fig. 7 as M_1, M_2, and H. The arrows indicate the positive directions of the forces and couples.

Figs. 7, (1), (2), (3) show the moment-areas for the structure as obtained from the Rahmenformeln for the self-stressed conditions $M_1 = -1$, $M_2 = -1$, $H = -1$,* respectively. By pairing the diagrams, as already explained, the

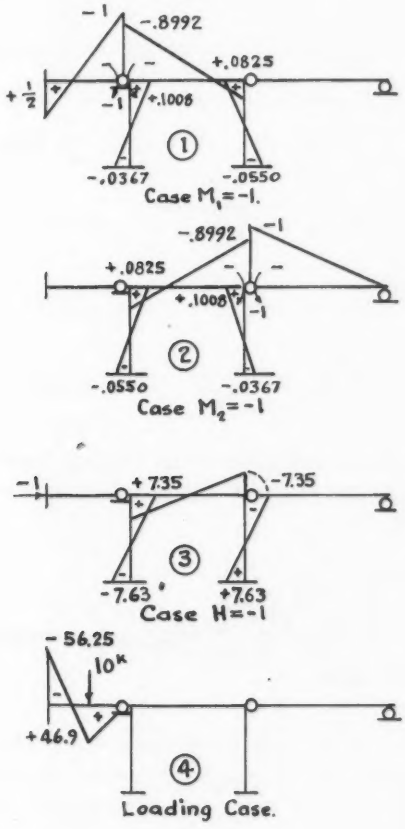

FIG. 7.

numerical coefficients are easily obtained. They are shown as elements of the matrix.

The equations have been solved for the simple case of loading shown in Fig. 7 (4). The reciprocal matrix for three equations is very easily obtained and once set down serves for all possible cases of loading and temperature changes.

* *Actually H is the connecting force, at the right-hand end, of the left span to the center span.*

$$\begin{bmatrix} 0.7927 & 0.1223 & -1.226 \\ 0.1223 & 0.5115 & 1.226 \\ -1.226 & 1.226 & 352.7 \end{bmatrix} \cdot \begin{bmatrix} M_1 \\ M_2 \\ H \end{bmatrix} = \begin{bmatrix} -19 \\ 0 \\ 0 \end{bmatrix}$$

$$\begin{bmatrix} M_1 \\ M_2 \\ H \end{bmatrix} = \frac{1}{135.4} \begin{bmatrix} 178.9 & -44.64 & 0.7770 \\ -44.64 & 278.1 & -1.122 \\ 0.7770 & -1.122 & 0.3905 \end{bmatrix} \cdot \begin{bmatrix} -19 \\ 0 \\ 0 \end{bmatrix}$$

$$M_1 = -\frac{3397.77}{135.3} = -25.1^{ft.k}$$

$$M_2 = +\frac{849.55}{135.3} = +6.27^{ft.k}$$

$$H = -\frac{14.763}{135.3} = -0.109^{k}$$

The final bending moment diagram for the loading chosen is shown in Fig. 8. The bending moment diagrams of Fig. 7 are used to determine the bending moment diagrams of Fig. 8.

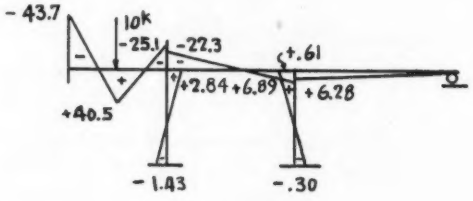

FIG. 8.

A second analysis of the same structure in which a cut has been made at the middle of the center span is shown in Figs. 9 and 10. The equations

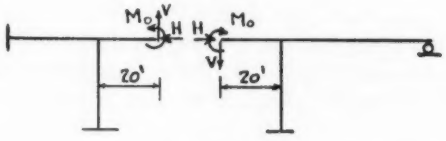

FIG. 9.

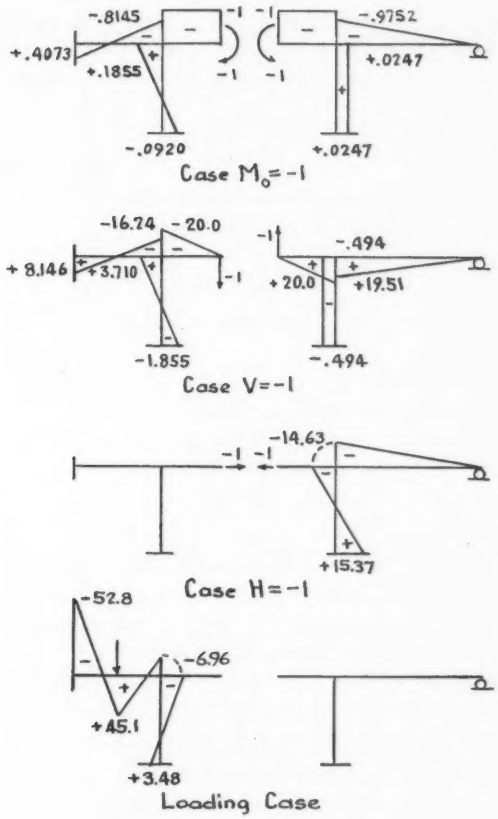

FIG. 10.

follow and the results shown in Fig. 11 check within reason those of the first analysis. All the numerical work, except for the final reciprocal matrix, was carried out on an ordinary slide rule.

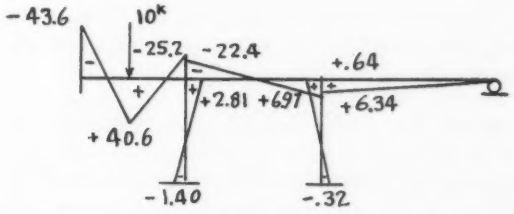

FIG. 11.

$$\begin{bmatrix} 1.632 & 3.814 & 3.309 \\ 3.814 & 385.9 & -66.18 \\ 3.309 & -66.18 & 718.4 \end{bmatrix} \cdot \begin{bmatrix} M_0 \\ V \\ H \end{bmatrix} = \begin{bmatrix} -15.5 \\ -310.0 \\ 0 \end{bmatrix}$$

$$\begin{bmatrix} M_0 \\ V \\ H \end{bmatrix} = \frac{1}{428.9} \begin{bmatrix} 272.9 & -2.959 & -1.529 \\ -2.959 & 1.162 & 0.1206 \\ -1.529 & 0.1206 & 0.6152 \end{bmatrix} \begin{bmatrix} -15.5 \\ -310.0 \\ 0 \end{bmatrix}$$

$$M_0 = -7.72^{ft.k}$$

$$V = -0.733^{k}$$

$$H = -0.0319^{k}$$

In cases of symmetrical structures, advantage should be taken of the symmetry that can be maintained by suitable choice of cuts or hinges. Also the method of group loadings can be used to advantage wherever group loadings tend to simplify the moment-area diagrams. By group loadings is meant the choice of two or more unit loads, or couples, applied to the primary structure simultaneously to produce a self-stressed condition. This method, however, does not reduce the number of redundants.

The method of the elastic center can be applied also by making the a_{ij}, $i \neq j$ coefficients equal to zero, but a preliminary investigation shows that, except in the case of symmetrical structures, there is little, if any, advantage to be gained by it.

Influence Lines

If further detailed study of the structure be required, influence lines should be drawn. This can be done by setting up the equations of the influence line for any chosen item that requires detailed attention.

As an illustration, let it be required to draw the influence line for M_1. In the solution, only the loading terms will change; therefore, the equation for M_1 will be, from the reciprocal matrix,

$$M_1 = 1.325C_1 - 0.331C_2 + 0.00574C_3, \qquad (1)$$

in which the C's are to be determined by pairing the moment-area diagram for the unit load with each of the moment-area diagrams for the three self-stressed conditions.

The moment-area diagrams for the unit load in each span successively are shown in Fig. 12. There will be one equation for each span. For Case *a*, only C_1 will be present and for Case *c*, only C_2. For Case *b*, however, all three values of C will exist.

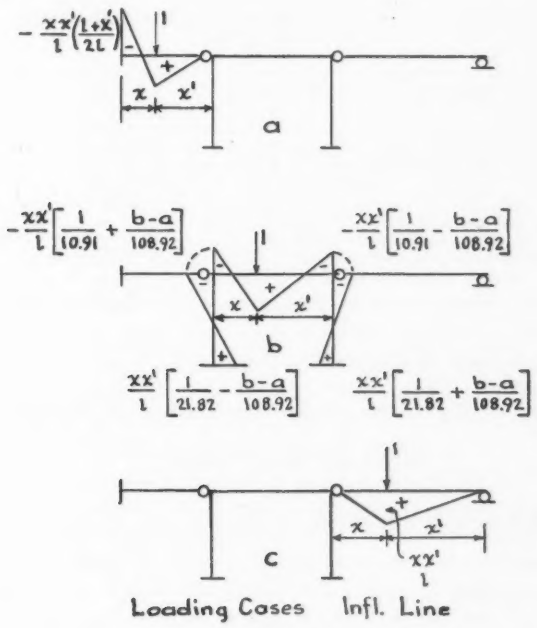

FIG. 12.

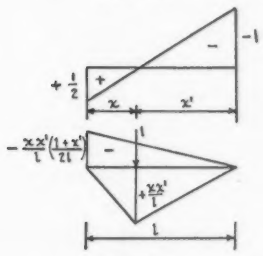

FIG. 13.

In order to express the position of the moving unit load, we shall take it at a distance x from the left-hand end of each span, and x' from the right-hand end. For the unit load on the left-hand span C_1 can be most readily obtained from Fig. 13. Thus, from pairing the moment-areas shown, we find

$$C_1 = \frac{-2.03x^2x'}{4l^2}$$

In a similar way we obtain for the center and the right-hand spans respectively

$$C_1 = \frac{xx'}{l}(-0.1107 - 0.1506b + 0.0146a)$$

$$C_2 = \frac{xx'}{l}(-0.1107 - 0.1506a + 0.0146b)$$

$$C_3 = \frac{xx'}{l}\,1.225\,(b - a),$$

and

$$C_2 = \frac{-0.1132\,xx'}{l^2}(l + x'),$$

in which

$$\frac{x}{l} = a, \qquad \frac{x'}{l} = b.$$

Inserting these values of C in Equation (1), we find for the three spans, respectively,

$$M_1 = -20.2\,a^2b$$

$$M_1 = -7.33\,ab - 7.85\,ab^2 + 2.49\,a^2b$$

$$M_1 = +1.87\,(a^2b + ab^2)$$

The plotted influence line is shown in Fig. 14.

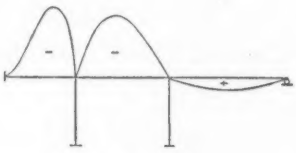

FIG. 14.

PRECISION OF HEAT TRANSFER MEASUREMENTS WITH THERMOCOUPLES—INSULATION ERROR[1]

W. A. MOHUN[2]

Abstract

A method has been developed for calculating the temperature variation in insulated thermocouple lead wires that do not follow an isothermal path. The difference between the temperature of the junction and that of the surrounding material that it purports to measure has been called "insulation error." It has been shown that insulation error is determined by variations in the temperature of the path followed by the lead wires only over a limited distance from the junction, which has been called the "critical distance." Hence, to eliminate insulation error the path of the wires need be isothermal only for the critical distance. A simple method has been developed for calculating the critical distance and the insulation error. When the path of the wires cannot be made isothermal the conditions for minimum experimental error are shown to be small diameter wires of low specific conductivity with a minimum of insulation.

The determination of fluid film heat transfer coefficients requires the measurement of the surface temperature of the tube or other dividing wall through which heat is being transferred. This usually requires that a thermocouple be embedded in the tube wall and the surface temperature calculated from the temperature indicated by the couple.

In a previous paper (1) the effects of geometric errors in determining the location of the thermocouple tip with respect to the tube surface were analyzed and methods of minimizing them were described. The other major source of error in such systems may be termed "insulation error" since it occurs when *insulated* lead wires are carried away from the junction along a path that is not isothermal. Heat is then transmitted to, or from, the junction along the wire itself so that the temperature of the junction is actually different from that of the material surrounding it. It has long been recognized qualitatively that the lead wires should be brought out along an isothermal path. But in practice it is not usually possible to adhere strictly to this condition, particularly in the case of tubes, for which chordal holes are preferably employed. It is hoped that the present quantitative analysis will help investigators, not only to estimate the magnitude of errors that cannot be avoided, but more particularly to choose experimental arrangements that will minimize these errors.

Qualitative Discussion

It is convenient to discuss the problem first in terms of a single insulated wire completely embedded in solid metal (e.g., in a low-melting solder) in a chordal hole in a tube wall, such as that in Fig. 1.

Heat will be flowing radially through the tube wall and the temperature gradient within the wall will depend on the density of heat flux and on the

[1] *Manuscript received July 8, 1948.*

[2] *Formerly Design Engineer, Chemical Engineering Section, National Research Council, Ottawa. Present address: Standard Chemical Company Ltd., Toronto, Ont.*

thermal conductivity of the wall. Table I shows that the temperature gradient in the wall may be quite steep and that the temperature difference across the width of a fine thermocouple lead wire may amount to several

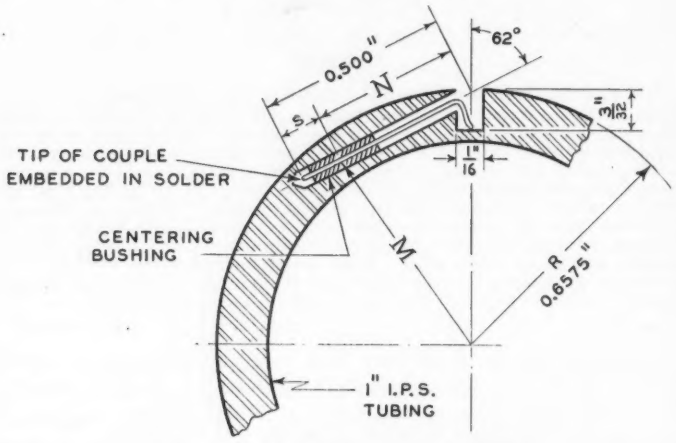

FIG. 1. *Sketch of thermocouple installation.*

TABLE I

TEMPERATURE GRADIENTS THROUGH METAL WALLS

Metal	k at 400° F.*, B.t.u./(hr.) (sq. ft.) (° F./in.)	Heat flux, B.t.u./(hr.) (sq. ft.)	Temp. gradient ° F./in.	Temp. difference (° F.) across	
				1 in. I.P.S. wall†	No. 30 B & S wire‡
Copper	2605	400,000	153	20.4	1.6
		200,000	77	10.2	0.8
		100,000	38	5.1	0.4
		50,000	19	2.6	0.2
Aluminum	1560	400,000	256	34.0	2.7
		200,000	128	17.0	1.3
		100,000	64	8.5	0.7
		50,000	32	4.2	0.3
Yellow brass	1010	400,000	396	52.6	4.2
		200,000	198	26.3	2.1
		100,000	99	13.2	1.0
		50,000	50	6.6	0.5
Steel	300	200,000	667	88.7	7.0
		100,000	334	44.4	3.5
		50,000	167	22.2	1.8

* *Kent, "Mechanical Engineers' Handbook", Vol. I, 3-28.*
† *Thickness = 0.133 in.*
‡ *Thickness = 0.0105 in.*

degrees. As a result of this temperature difference across the wire, heat will flow through the insuiation into the wire, across the wire, and out again through the insulation on the other side. Because of the high thermal resistance of the electrical insulation, the amount of heat that takes this path will be small relative to the flux through the tube wall itself, but it may not be negligible. Furthermore, if the wire is not isothermal along its length, some of the heat that enters through the insulation at a given point will flow along the wire before passing out through the insulation on the other side. The components of flow across the wire and along the wire may be considered separately. The former component is not of major importance in the present discussion as it does not alter the temperature of the wire, but the component along the wire causes the temperature of the wire to differ from that of its immediate surroundings, and is the cause of insulation error.

The first conclusions of importance will be made clear by reference to Figs. 2 and 3, which illustrate a wire subjected only to a transverse component of heat flux. Fig. 2 shows a cross section of the tube and wire in the plane

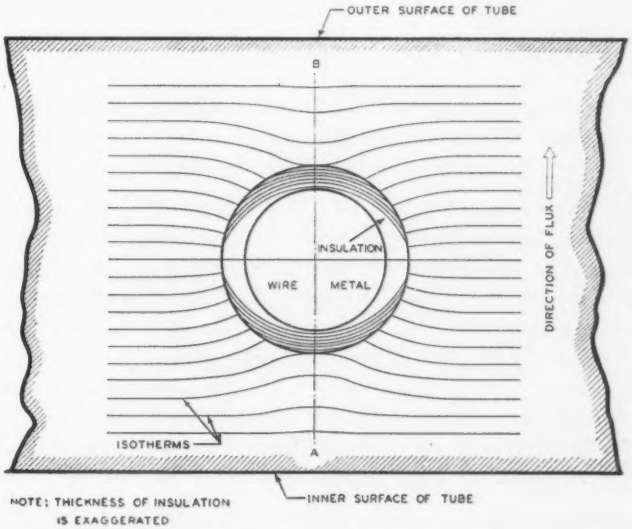

FIG. 2. *Enlarged cross section of tube in plane of heat flux showing distortion of isotherms by insulated wire—for case of no longitudinal heat flux.*

of the heat flux; this is a longitudinal section in the case of the tube; for simplicity throughout this paper it will be assumed to be a right cross section in the case of the wire, although strictly speaking the axis of the wire is not necessarily normal to the radii of the tube, so that cross sections of the wire in the plane of the heat flux may actually be slightly elliptical in shape. This figure illustrates roughly how the isotherms, normally parallel, are

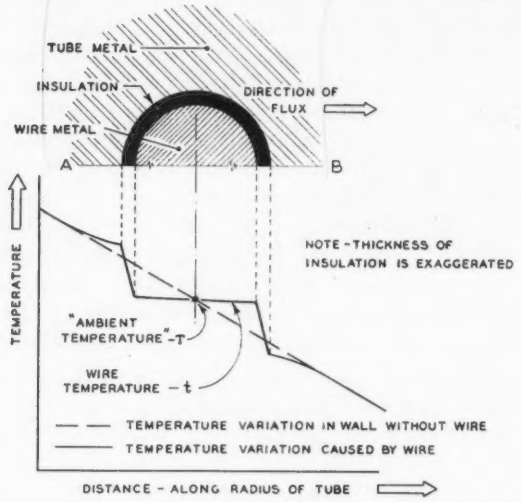

FIG. 3. *Temperature variation across wire—for case of no longitudinal heat flux.*

distorted in the region of the wire. Temperatures along the line AB of Fig. 2, a line which passes through the center of the wire, are plotted against distance in Fig. 3. From these figures we may draw two conclusions:

(*a*) The temperature drop is so largely concentrated in the insulation that the temperature of the wire metal may be considered essentially constant across any given cross section taken in the direction of heat flow; this wire temperature at any given point will be called t. Then let T be the temperature that would have obtained in the metal wall at the same point (corresponding to the center of the wire) if the wire had not been there. This "would-have-been" temperature is the average of the actual temperatures existing in practice on the two sides of the wire (see Fig. 3), and, since it is thus the average temperature to which the periphery of the wire at any cross section is subjected, it will be termed the *ambient* temperature.

(*b*) Assuming that the cross section of the wire and its insulation is symmetrical and that the temperature gradient in the surrounding metal wall is uniform, we see from Fig. 3 that $t = T$ when there is no longitudinal distribution of heat.

But when the wire is not brought out along an isothermal path, heat flows along the wire as well as across it, and t is no longer equal to T. Then at the tip of the wire (i.e., at the junction):

$$\text{Insulation error} = t_0 - T_0 . \qquad (1)$$

Insulation Temperature Drop

At any given cross section of the wire, the temperature of the outer surface of the insulation varies from a maximum on the side nearest the inside of the tube to a minimum on the side nearest the outside of the tube. Since the temperature variation in the tube wall is linear with distance if one neglects distortion of the isotherms in the immediate region of the wire, the projection of the peripheral temperature on the diameter will, to a first approximation, also be linear with distance (see Fig. 4, and compare with Fig. 3). In Fig. 4,

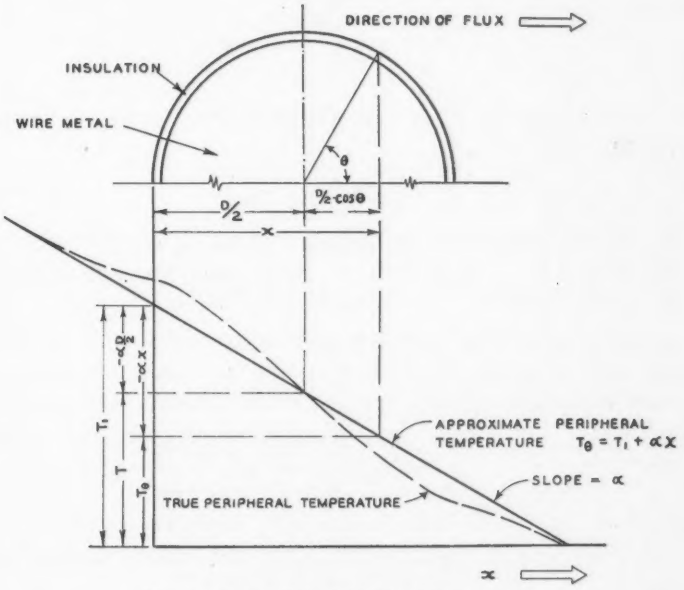

FIG. 4. *Calculation of peripheral temperature.*

x is distance measured across the diameter of the wire from the hotter side, α is the temperature gradient in the tube wall,* and T_θ is the temperature at any point on the periphery of the wire. From the geometry of Fig. 4 it follows that

$$T = T_1 + \frac{\alpha D}{2} ; \tag{2}$$

and,

$$T_\theta = T_1 + \frac{\alpha D}{2} + \frac{\alpha D}{2} \cos \theta . \tag{3}$$

Since the temperature of the wire metal may be considered essentially constant throughout the cross section, the temperature difference across the insulation at any point around the periphery is

$$\Delta T_i = T_\theta - t . \tag{4}$$

* *Since the temperature decreases in the positive direction of x, α is negative.*

This temperature difference ΔT_i is not constant around the wire, but varies from a maximum positive value at one side of the wire to a maximum negative value at the other side. When the positive and negative values of ΔT_i are symmetrical and equal, the quantities of heat entering and leaving the wire at the cross section are equal and there is no flow of heat along the wire. When the positive and negative values are not equal, the effective ΔT_i causing a net flow of heat into the wire is the average value of ΔT_i taken around the periphery of the wire; that is,

$$\overline{\Delta T_i} = \frac{1}{\pi}\int_0^{\pi} \Delta T_i \, . \, d\theta \, . \tag{5}$$

Substituting from Equations (4) and (3), integrating, and then substituting Equation (2):

$$\overline{\Delta T_i} = T - t \, . \tag{6}$$

That is, the average temperature difference causing a net flow of heat into, or out of, the wire at any given cross section is simply the difference between the ambient temperature and the temperature of the wire.

It can be seen intuitively that Equation (6) is not restricted to the hypothetical case in which T_θ is a linear function of x; the integration will give the same result provided only that T_θ is symmetrical with respect to T at the center of the wire. This condition, and hence Equation (6), may be assumed to be approximately true at any cross section of the wire (see dotted curve in Fig. 4), although this condition is rigorously true only in the limiting case when the fluxes entering and leaving the wire at the same cross section are equal, i.e., when there is no longitudinal flux and t equals T, as illustrated in Fig. 3.

Wire Temperature Equation

In order to obtain an expression defining the temperature of the wire metal at any point, consider an increment of the wire taken as a right cross section, ds inches thick, at a distance s from the tip, as shown in Fig. 5. In general, the direction of increasing temperature in the wire metal will be the same as the direction of increasing ambient temperature, since it is the change in ambient temperature that causes change in wire temperature. The ambient temperature will be some function of s, and for convenience the temperature datum will be taken as zero ambient temperature at the tip of the wire. Consider the flow of heat Q through the cross section at s into the part of the wire to the left of the section as the positive direction of heat flux, since this has been arbitrarily defined in Fig. 5 as being the direction of decreasing wire temperature.

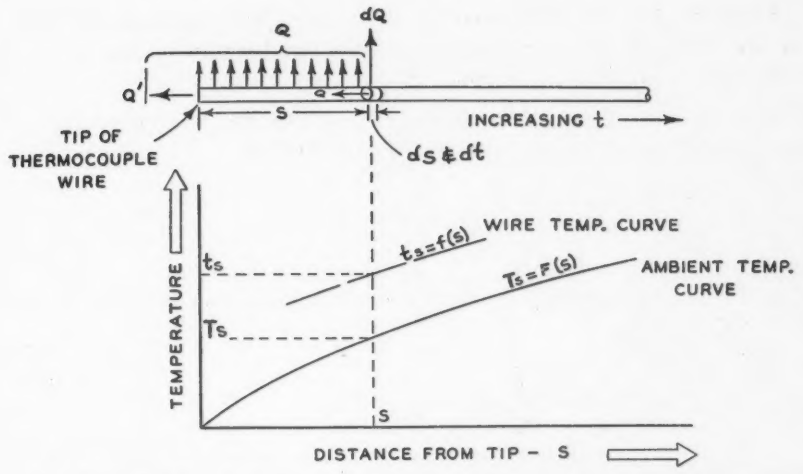

FIG. 5. *Calculation of wire temperature equation for known ambient temperature curve.*

Then according to Newton's law the flow of heat across the increment is given by

$$Q = -K \cdot \frac{\pi D^2}{4} \frac{dt}{ds}, \tag{7}$$

where the symbols are as defined in the Table of Nomenclature.

Since the flow of heat out through the surface of the increment is

$$dQ = \frac{k}{w} \cdot \pi D \cdot ds(T - t) , \tag{8}$$

the heat lost through the surface and end of the wire will be

$$Q = \int_0^S dQ + Q'$$

$$= \frac{k\,\pi D}{w} \int_0^S (T - t)ds + \frac{k}{w} \cdot \frac{\pi D^2}{4} (T_0 - t_0) . \tag{9}$$

Since heat is not stored in any part of the wire, we may equate (7) and (9), and noting that $T_0 = 0$ by definition we obtain

$$\int_0^S \phi \cdot T \cdot ds - \int_0^S \phi \cdot t \cdot ds - \frac{k\,t_0}{wK} = -\frac{dt}{ds}, \tag{10}$$

where $$\phi = \frac{4k}{wKD}, \tag{10a}$$

and dt/ds is the temperature gradient in the wire at s.

Equation (10) defines the curve $t = f(s)$ giving the temperature of the wire at any point. In practice ϕ may differ for different regions along the length of the wire, so it is best to keep it inside the integral sign.

Since the heat Q' lost through the end of the wire may usually be neglected, as will be shown later, Equation (10) may be written

$$\int_0^S \phi \,.\, T \,.\, ds - \int_0^S \phi \,.\, t \,.\, ds = -\frac{dt}{ds}. \tag{11}$$

And for a value s' corresponding to a maximum or a minimum in the curve $t = f(s)$, we have

$$\int_0^{S'} \phi \,.\, T \,.\, ds - \int_0^{S'} \phi \,.\, t \,.\, ds = 0 \,. \tag{12}$$

Equation (12) indicates that the wire may be considered divided into separate regions by the maxima and minima in the t curve, and that temperature effects in one region do not carry over into the next. It is also evident that the maxima and minima in the curve $t = f(s)$ coincide with the maxima and minima in the curve $T = F(s)$ since the variations in t are due solely to the variations in T and hence must always be in the same sense as those in T. This generalization is helpful in plotting the wire temperature curve, and makes Equation (12) applicable where s' is defined by the maxima and minima in the ambient temperature curve.

Equation (11) cannot be solved directly to determine the wire temperature curve, but Equations (11) and (12) provide the criteria by which we may check any wire temperature curve obtained by trial and error or approximate methods.

Approximate Solution

An approximate solution of Equation (10), sufficiently accurate for all practical purposes, may be obtained by converting it to the approximate form

$$\int_0^S \phi \,.\, T \,.\, ds - \Sigma_0^n \phi \,.\, \bar{t} \,.\, \Delta s - \frac{k\, t_0}{wK} = -\frac{\Delta t_n}{\Delta s_n}, \tag{13}$$

where $\bar{t}$ is the average value for each increment concerned.

If each increment is assumed to be sufficiently small that the variation in t across it may be considered linear with distance, we may write

$$\bar{t}_n = t_{n-1} + \frac{\Delta t_n}{2} \tag{14}$$

for any increment. Using Equation (14), the second term of Equation (13) may be broken up into some of its constituent increments, so that Equation (13) becomes

$$\int_0^S \phi \,.\, T \,.\, ds - \Sigma_0^{n-2} \phi \,.\, \bar{t} \,.\, \Delta s - \phi_{n-1} \,.\, \Delta s_{n-1} \left(t_{n-2} + \frac{\Delta t_{n-1}}{2} \right)$$

$$- \phi_n \,.\, \Delta s_n \left(t_{n-2} + \Delta t_{n-1} + \frac{\Delta t_n}{2} \right) - \frac{k\, t_0}{wK} = - \frac{\Delta t_n}{\Delta s_n} . \qquad (15)$$

The significance of the various subscripts will be made clear by reference to Fig. 6.

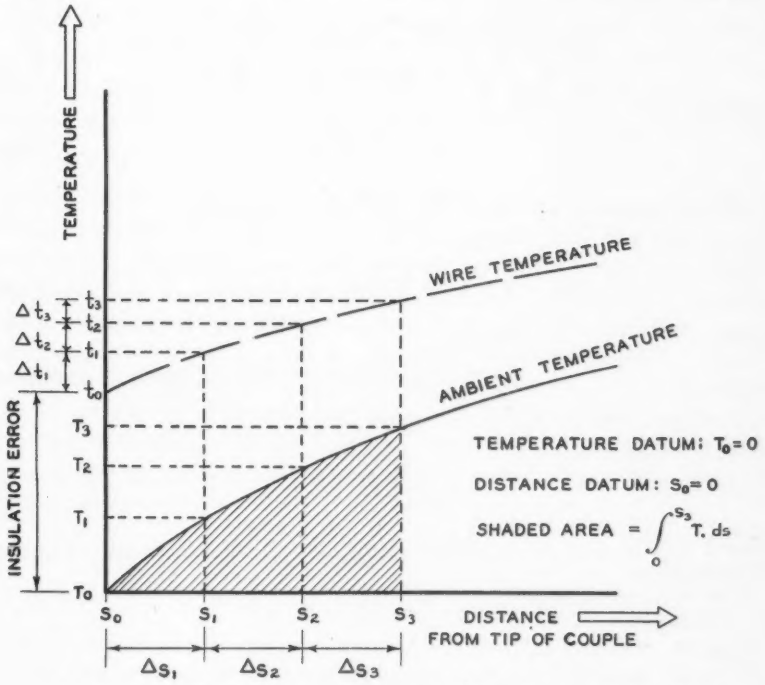

FIG. 6. *Sketch illustrating approximate solution of wire temperature equation.*

Regrouping, letting $\Delta s_n = \sqrt{2/\phi_n}$ so that the term containing Δt_n disappears, and solving for Δt_{n-1}, we obtain

$$\Delta t_{n-1} = \frac{2}{\phi_{n-1} \,.\, \Delta s_{n-1} + 2\phi_n \,.\, \Delta s_n} \left[\int_0^S \phi \,.\, T \,.\, ds - \Sigma_0^{n-2} \phi \,.\, \bar{t} \,.\, \Delta s \right.$$

$$\left. - t_{n-2} \left(\phi_{n-1} \,.\, \Delta s_{n-1} + \phi_n \,.\, \Delta s_n \right) - \frac{k\, t_0}{wK} \right], \qquad (16)$$

in which

$$\Delta s_n = \sqrt{2/\phi_n} \,. \tag{16a}$$

Equation (16) may be used to calculate Δt for each increment in turn except the first. For example, when $n = 2$, and for a case in which $\phi_1 \,.\, \Delta s_1 = \phi_2 \,.\, \Delta s_2$, Equation (16) reduces to

$$\Delta t_1 = \frac{0.667}{\phi \,.\, \Delta s}\left[\int_0^{s_2} \phi \,.\, T \,.\, ds - 2\phi \,.\, \Delta s \,.\, t_0 - k \,.\, t_0/w \,.\, K\right]. \tag{17}$$

For the first increment, $n = 1$, and Equations (13) and (14) may be combined and reduced to

$$\int_0^{s_1} \phi \,.\, T \,.\, ds - \phi_1 \,.\, \Delta s_1 \,.\, t_0 - \frac{k\, t_0}{wK} = 0 \,, \tag{18}$$

in which

$$\Delta s_1 = \sqrt{2/\phi_1} \,. \tag{18a}$$

Dividing through by $\phi_1 \,.\, \Delta s_1 = \dfrac{4k \,.\, \Delta s_1}{wKD}$, and regrouping

$$t_0\,(1 + E) = \frac{1}{\phi_1 \,.\, \Delta s_1}\int_0^{s_1} \phi \,.\, T \,.\, ds \tag{19}$$

where

$$E = \frac{D}{4\,\Delta s_1} \text{ is the correction for heat passing through the end area of the wire,}$$

$$= \sqrt{\frac{D\,k}{8wK}} \,. \tag{20}$$

When $T = F(s)$ may be considered linear over the first increment, Equation (19) reduces to

$$t_0 \simeq \frac{1}{2}\, T_1/(1 + E) \,. \tag{21}$$

Value of E

Table II lists thermal conductivities of materials commonly used for electrical insulation; the conductivity of copper wire in the same units is about unity. For purposes of illustration, we will assume an average value of $k/K = 5.0 \times 10^{-4}$.

Assuming No. 30 B & S enamelled wire with a diameter of 0.0105 in. outside the insulation and a diameter of 0.0100 in. for the bare wire, the thickness of the insulation may be taken as $w = 0.00025$ in. These values may readily be determined with a traveling microscope in the case of the

TABLE II

THERMAL CONDUCTIVITIES OF INSULATING MATERIALS

10^{-4} cal./(sec.) (sq. cm.) (°C./cm.)

Polyvinyl formal	3.7
Vinyl chloride-acetate	3.9 – 4.0
Rubber	4.3 – 4.5
Gutta percha	4.8
Varnished cloth	5.2
Polyethylene	6.0 – 8.0

Authorities: Miner, "Insulation of Electrical Apparatus," McGraw-Hill, 1941. "Plastics Catalogue," 1946. "Handbook of Physics and Chemistry."

original wire insulation. It is more difficult to estimate the thickness of insulation such as Heresite applied over the tip after soldering the thermocouple.

For such a wire, $E = 0.05$, by Equation (20).

It is evident, therefore, that neglecting the term $(1 + E)$ in Equation (19) or (21) will, in the present example, introduce an error of only 5%, which is so much less than the error that would normally be encountered in estimating k and w for the insulation, that this factor E, to allow for heat entering the wire through its end area, may be neglected. With an equally negligible error the corresponding term $k \cdot t_0/w \cdot K$ may be neglected in the equations where it occurs. It is obvious that there may be cases, particularly with thicker wires, in which E is not negligible, but for simplicity this end effect will be neglected throughout the rest of this paper. Then Equations (1) and (21) reduce to:

$$\text{Insulation error} = t_0 \approx T_1/2 \; . \tag{22}$$

Calculation of Ambient Temperature

The method of calculating the ambient temperature depends, of course, upon the geometry of the thermocouple arrangement employed. Since the case of the chordal hole shown in Fig. 1 is similar to many arrangements commonly used, the ambient temperature curve has been calculated from the tip of the couple to the thermocouple groove. It was assumed that the tip of the couple is 0.500 in. from the surface measured along the axis of the hole, and that the wire is bent down from the axis of the hole at a distance of 0.45 in. from the tip, reaching the bottom of the groove at $s = 0.55$ in. from the tip. The bottom of the groove itself was assumed relatively isothermal over moderate distances, and the flux was taken such as to produce a temperature gradient of 50° F. per inch in the metal wall of the tube.

From the geometry of Fig. 1 it will be obvious that

$$M = \sqrt{N^2 + R^2 - 2N.R.\cos 62°}$$

where

$$N = 0.500 - s\ ;$$

and that

$$T = 50\,(0.6112 - M)\ .$$

The calculated values are shown in Table III and the resulting ambient temperature curve is shown in Fig. 7. This typical ambient temperature curve will be used to illustrate the calculation of wire temperature.

TABLE III

CALCULATION OF AMBIENT TEMPERATURE

Distance from tip s, in.	M, inches	Ambient temperature, T, ° F.
0.00	0.6112	0.00†
0.05	0.5975	0.68
0.10	0.5877	1.18
0.15	0.5820	1.46
0.20	0.5806	1.53
0.25	0.5835	1.38
0.30	0.5906	1.03
0.35	0.6018	0.47
0.40	0.6169	−0.28
0.45	0.6356	−1.22
0.55*	0.5638	2.37

† *Temperature datum.*

* *At bottom of groove, 0.0937 in. deep; $M = 0.6575 - 0.0937$.*

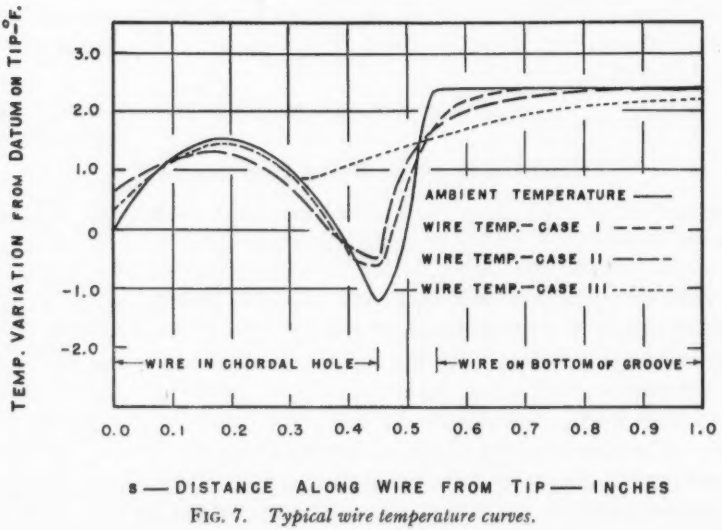

FIG. 7. *Typical wire temperature curves.*

Calculation of Wire Temperature

In order to give a better understanding of the phenomena involved, the wire temperature has been calculated for three typical cases and the calculations have been carried to several significant figures so that the trends will be clearly shown. The calculation consists of a stepwise solution, one increment at a time, proceeding along the wire from its tip.

Case I

Assume that the insulation throughout the length of the wire is equivalent to the original insulation, 0.00025 in. thick.
Then $\phi = 800$ in.$^{-2}$ by Equation (10a);

$$\Delta s = \sqrt{2/800} = 0.05 \text{ in.; and } \phi \cdot \Delta s = 40 \text{ in.}^{-1}$$

The calculations are tabulated in Table IV and the resulting wire temperature curve is plotted in Fig. 7. For the first increment one uses the simplified form of Equation (19), in which end effect is neglected:

$$t_0 = \frac{1}{\phi \cdot \Delta s} \int_0^{s_1} \phi \cdot T \cdot ds \ . \tag{23}$$

And for the second increment one uses the similarly simplified form of Equation (17):

$$\Delta t_1 = \frac{0.667}{\phi \cdot \Delta s} \left[\int_0^{s_2} \phi \cdot T \cdot ds - 2\phi \cdot \Delta s \cdot t_0 \right] . \tag{24}$$

For subsequent increments Equation (16), simplified because $\phi \cdot \Delta s$ is constant, is used in the form

$$\Delta t_{n-1} = \frac{0.667}{\phi \cdot \Delta s} \left[\int_0^{s} \phi \cdot T \cdot ds - \Sigma_0^{n-2} \phi \cdot \bar{t} \cdot \Delta s - 2\phi \cdot \Delta s \cdot t_{n-2} \right] . \tag{25}$$

The first step in the calculation is to fill in the part of the table to the left of the double line, which involves integrating the area under the ambient temperature curve for each increment. In the present work the integration was performed by the primitive but nonetheless satisfactory method of counting squares on the graph paper under the curve in Fig. 7. One then proceeds by working across the table from left to right, completing each line before dropping down to the next. If this systematic procedure is followed, what can be a rather confusing calculation becomes quite straightforward.

As a check on the calculations of Case I, we may apply the criterion provided by Equation (12). The first maximum in the ambient temperature curve occurs at $s = 0.191$ (approx. $n = 4$), and the minimum occurs at $s = 0.450$ ($n = 9$). Applying the criterion, for the first maximum:

$$\int_0^{s_4} \phi \cdot T \cdot ds - \Sigma_0^4 \phi \cdot \bar{t} \cdot \Delta s = 166.24 - 167.38 = -1.14,$$

and similarly, for the minimum:

$$\int_0^{s_9} \phi \,.\, T \,.\, ds - \Sigma_0^9 \phi \,.\, \bar{t} \,.\, \Delta s = 280.56 - 275.20 = 5.36 \,.$$

TABLE IV

CALCULATION OF WIRE TEMPERATURE CURVE

n	s_n	T_n	$\int_0^s \phi . T . ds$	Δt_{n-1}	t_{n-1}	$\phi . \Delta s . \bar{t}_{n-1}$	$\Sigma_0^{n-1} \phi . \bar{t} . \Delta s$	$2\phi . \Delta s . t_{n-1}$
Case I								
1	0.05	0.68	14.04	—	0.351	—	—	28.08
2	0.10	1.18	51.88	0.397	0.748	22.00	22.00	59.84
3	0.15	1.46	105.52	0.395	1.143	37.82	59.82	91.44
4	0.20	1.53	166.24	0.250	1.393	50.72	110.54	111.44
5	0.25	1.38	225.32	0.056	1.449	56.84	167.38	115.92
6	0.30	1.03	274.48	−0.147	1.302	55.02	222.40	104.16
7	0.35	0.47	305.40	−0.353	0.949	45.02	267.42	75.92
8	0.40	−0.28	309.92	−0.557	0.392	26.82	294.24	31.36
9	0.45	−1.22	280.56	−0.751	−0.359	0.66	294.90	− 28.72
10	0.50	0.10	250.16	−0.267	−0.626	−19.70	275.20	− 50.08
11	0.55	2.37	306.04	1.349	0.723	1.94	277.14	57.84
12	0.60	2.37	400.84	1.098	1.821	50.88	328.02	145.68
13	0.65	2.37	495.64	0.366	2.187	80.16	408.18	174.96
14	0.70	2.37	590.44	0.122	2.309	89.92	498.10	184.72
15	0.75	2.37	685.24	0.040	2.349	93.16	591.26	187.92
16	0.80	2.37	780.04	0.014	2.363	94.24	685.50	189.04
17	0.85	2.37	874.84	0.005	2.368	94.62	780.12	189.44
18	0.90	2.37	969.64	0.001	2.369	94.74	874.86	—
Case II								
1	0.10	1.18	12.97	—	0.648	—	—	25.92
2	0.20	1.53	41.56	0.521	1.169	18.17	18.17	46.76
3	0.30	1.03	68.62	0.123	1.292	24.61	42.78	51.68
4	0.40	−0.28	77.48	−0.566	0.726	20.18	62.96	29.04
5	0.50	0.10	62.54	−0.982	−0.256	4.70	67.66	− 10.24
6	0.60	2.37	100.21	1.426	1.170	9.14	76.80	46.80
7	0.70	2.37	147.61	0.800	1.970	31.40	108.20	78.80
8	0.80	2.37	195.01	0.267	2.237	42.07	150.27	89.48
9	0.90	2.37	242.41	0.089	2.326	45.63	195.90	93.04
10	1.00	2.37	289.81	0.029	2.355	46.81	242.71	94.20
11	1.10	2.37	337.21	0.010	2.365	47.20	289.91	94.60
12	1.20	2.37	384.61	0.003	2.368	47.33	337.24	—
**Case III*								
1	0.05	0.68	14.04	—	0.351	—	—	28.08
2	0.10	1.18	51.88	0.397	0.748	22.00	22.00	59.84
3	0.15	1.46	105.52	0.395	1.143	37.82	59.82	91.44
4	0.20	1.53	166.24	0.250	1.393	50.72	110.54	111.44
5	0.25	1.38	225.32	0.056	1.449	56.84	167.38	115.92
6	0.30	1.03	274.48	−0.147	1.302	55.02	222.40	104.16
7	0.35	0.47	305.40	−0.353	0.949	45.02	267.42	—
8	0.666	2.37	310.92	−0.017	0.932	37.62	305.04	11.78
9	0.982	2.37	325.90	0.958	1.890	8.92	313.96	23.89
10	1.298	2.37	340.88	0.320	2.210	12.96	326.92	27.93
11	1.614	2.37	355.86	0.107	2.317	14.31	341.23	29.28
12	1.930	2.37	370.84	0.035	2.352	14.76	355.99	—

* *Case III is identical with Case I down to the heavy line at $s_n = 0.35$, at which point the increase in insulation thickness occurs.*

The figure 1.14 is an error of 0.7% at the first maximum, and 5.36 is an error of 2% at the minimum. These errors are primarily due to the assumption on which Equation (14) is based, namely, that the wire temperature curve may be considered linear over the length of each increment. It will be noted that the error introduced by this assumption is not large. An increase in Δs would tend to increase this error, but when an increase in Δs corresponds to an increase in the amount of insulation it tends to make the curve flatter and thereby has a compensating effect.

Case II

Assume that the insulation throughout the length of the wire is 0.001 in. thick. Then $\phi = 200$; $\Delta s = 0.10$; $\phi.\Delta s = 20$.

The calculations here are identical with those for Case I and are as shown in Table IV. The resulting wire temperature curve shown in Fig. 7 indicates the effect of a four-fold increase in insulation thickness as compared with Case I.

It is interesting at this point to compare the values of insulation error obtained by the approximate equation (22) with those obtained by the more accurate form (23). For Case II the approximate equation gives an insulation error $t_0 = 1.18/2 = 0.590°$ F. compared with the more accurate value of 0.648° F., an error of 9%. For Case I the corresponding figures are 0.340 and 0.351, an error of 3%. It is obvious, therefore, that the approximate form (Equation 22) may only be used when Δs is relatively short, that is, when the insulation is quite thin.

Case III

Assume the case, illustrated in Fig. 1, in which the insulation thickness is 0.00025 in. from the tip of the wire to the back of the centering bushing—a distance that may be taken as 0.35 in.; and assume that the air or insulation in the drilled hole back of the bushing is equivalent to an insulation thickness of 0.01 in. This case is similar to the installation described in the previous paper (1) and is, therefore, typical of what may be encountered in practice.

The first part of the calculations is identical with that for Case I. For the second section of the wire, $\phi = 20$; $\Delta s = 0.316$; and $\phi.\Delta s = 6.32$. These calculations are also tabulated in Table IV. In the transition from one region to the other, care must be taken to use the correct values of ϕ and of Δs in the equations. Equation (16) must be used for calculating Δt_7, and $\phi.\Delta s = 40$ must be used in calculating $\phi.\Delta s \,.\, t_7$. Otherwise the procedure is identical with that employed for Cases I and II.

Critical Distance

An examination of Fig. 7 shows that the wire temperature approaches the temperature of the thermocouple groove more slowly the thicker the insulation. Similarly, disturbances in the ambient temperature (such as the minimum at $s = 0.45$) have less effect on wire temperature when the insula-

tion is thicker, and the disturbance in wire temperature is then distributed along a greater length of the wire. This indicates qualitatively the fact that the distance along the wire that a disturbance in ambient temperature is transmitted is some function of the thermal resistance of the insulation; it would also be expected to be a function of the conductivity of the wire.

Combining Equations (10*a*) and (16*a*) gives just such a relation, namely,

$$\Delta s = \sqrt{\frac{w}{k} \cdot \frac{KD}{2}}, \tag{26}$$

for w/kD is proportional to the thermal resistance of the insulation per unit length of wire, and KD^2 is proportional to the conductivity of the wire per unit of length. We therefore see illustrated what has already been demonstrated by the mathematics of the analysis, namely, that Δs defines the maximum distance that a disturbance at a specific point can be transmitted along the wire. Δs will, therefore, be called the "critical distance."

The significant conclusion is, therefore, reached that the path of the lead wires from the junction need be isothermal only for the critical distance; and if the path is not quite isothermal, then the insulation error is determined by the variation in ambient temperature only over the critical distance.

For Cases I and II above, the critical distances are 0.05 in. and 0.10 in., which are surprisingly short. It is obvious from Equation (26) that the critical distance, and hence the insulation error, is larger, the larger the thermal resistance, w/k, of the insulation. It follows, therefore, that experimenters should strive for a minimum of thermal insulation on the thermocouple wires near the tip without losing the necessary* electrical insulation. Under most circumstances an unusually thick blob of insulation on the tip of a thermocouple could seriously affect the accuracy of the readings. Other factors that will tend to reduce insulation error are small wire diameter and low specific conductivity of wire metal.

Effect of Joining Dissimilar Wires

The discussion thus far has been in terms of a single wire, whereas a thermocouple consists of two dissimilar wires, having different values of K and perhaps of D. Applying Equation (23) will, therefore, give different values, t_0' and t_0'', for the two wires. Since the wires are in thermal contact at the tip, their tip temperatures must be identical. In order to establish this equality heat will flow from the wire that is the better conductor into the poorer conductor and the tips will assume a temperature t_0 that is intermediate between t_0' and t_0'', the temperature differences being inversely proportional to the conductivities of the wires, thus:

$$\frac{t_0' - t_0}{t_0 - t_0''} = \frac{K''(D'')^2}{K'(D')^2}.$$

**It is, of course, possible to consider the use of a thermocouple with no insulation at the tip. But insulation simplifies testing; and it is the author's impression that insulated couples are more reliable, although he does not wish to be dogmatic on this point.*

Solving this equation gives

$$t_0 = \frac{K_1'(D')^2 t_0' + K''(D'')^2 t_0''}{K'(D')^2 + K''(D'')^2} . \tag{27}$$

For purposes of illustration constantan may be assumed to have a conductivity one-twentieth that of copper. Consider a copper–constantan thermocouple in which both wires are identical in size and insulation, the values being as in Case I preceding. Then $t_0' = 0.351°$ F. for copper (from Table IV), and $K' = 1.00$.

For the constantan wire $\phi = 16{,}000$; $\Delta s = 0.01118$;

$$\int_0^{s_1} \phi \, . \, T \, . \, ds = 13.5; \; t_0'' = 0.075° \text{F.}; \text{ and } K'' = 0.05.$$

Then $t_0 = \dfrac{0.351 + 0.05(0.075)}{1.00 + 0.05} = 0.338°$ F.

It is evident from the foregoing that, when the thermocouple wires differ greatly in conductivity, the temperature of the junction approaches very closely to that calculated for the better conductor alone. By conductivity is here meant the combined effect of specific conductivity and cross sectional area.

Conclusion

The error in indicated thermocouple temperature due to the presence of the insulation may be eliminated by arranging that the wires follow an isothermal path for a distance from the junction that need not be greater than the critical distance. When the path of the wires is not isothermal the resulting insulation error is determined by the variations in the ambient temperature only over the critical distance from the junction. The magnitude of this critical distance is determined by the relative capacities of the insulation and of the wire metal to conduct heat. The conditions for minimum insulation error are small wire diameter, low specific conductivity of wire metal, thin insulation, and high specific conductivity of the insulation material.

The calculations involved in plotting much of the curve of wire temperature are quite laborious, but are, fortunately, not usually necessary. The calculation of insulation error only is a relatively simple process, the necessary steps being as follows:

(*a*) Calculate the critical distance by Equation (26);

(*b*) From the geometry of the installation, calculate the ambient temperature T_1 at the critical distance from the junction;

(*c*) Calculate insulation error, $t_0 = T_1/2$.

The above procedure assumes that the ambient temperature curve is approximately linear over the critical distance. If greater accuracy is desired the procedure would be:

(*a*) Calculate the critical distance by Equation (26);

(*b*) From the geometry of the installation, calculate and plot the ambient temperature curve for a little more than the critical distance from the junction;

(*c*) With a planimeter or by counting squares, determine the area under the ambient temperature curve for the critical distance from the junction;

(*d*) Calculate insulation error, $t_0 = \frac{1}{\Delta s}\int_0^{\Delta s} T.\,ds$.

The calculated insulation errors in the examples used in this paper have been relatively small since they were based on cases in which insulation thickness and wire diameter were about ideal and since they were for a moderate temperature gradient of 50° F. per inch in the tube wall. Reference to Table I will show that gradients 5 to 10 times as steep may be encountered, giving under the best of conditions insulation errors of the order of a few degrees. Although insulation error is usually not as critical as the geometric errors described in the previous paper (1), it can be excessive if adequate precautions are not taken.

It is hoped that, in the future, authors reporting the results of heat transfer film coefficient measurements will calculate and report the values of geometric and insulation errors so that the accuracy of their data will be established.

Table of Nomenclature

D = diameter of thermocouple lead wire.

E = term to correct for heat entering end area of wire.

k = specific conductivity of wire insulation.

K = specific conductivity of wire metal.

M = distance from center of tube to any given point in the wire.

N = distance from surface of tube to same point in the wire as defines M, see Fig. 1.

Q = quantity of heat flowing across any given cross section of the wire.

Q' = quantity of heat flowing into wire through its end area.

R = radius of the tube.

s = distance measured along the thermocouple wire.

Δs = length of increment of wire; more specifically, Δs is "critical distance" = $\sqrt{2/\phi}$.

t = temperature at any given point in the thermocouple wire, i.e. "wire temperature."

$\bar{t}$ = average value of t for any given increment of the wire.

t_0 = wire temperature at the tip or junction; by choice of temperature datum t_0 is also equal to the insulation error.

T = average temperature of the surrounding tube metal to which any given cross section of the wire is subjected, i.e., "ambient temperature."

T_0 = ambient temperature at the tip or junction; $T_0 = 0$ by choice of datum temperature.

T_1 = ambient temperature at a distance $\Delta s_1 = \sqrt{2/\phi}$ from the tip or junction.

T_θ = temperature at any point on the periphery of the wire.

ΔT_i = temperature difference across the insulation of the wire at any point on its periphery; $\overline{\Delta T_i}$ is average of values around the periphery at any given cross section.

x = distance measured across the diameter of the wire from the hotter side.

w = thickness of wire insulation.

α = temperature gradient in the tube wall.

ϕ = a coefficient defined by Equation (10a)

θ = angle defining position of a point on periphery of wire, see Fig. 3

Primes: $'$ and $''$ indicate different values for two dissimilar metals forming a thermocouple, e.g., for copper and for constantan.

Acknowledgment

The author wishes to acknowledge his indebtedness to Mr. W. S. Peterson for assistance in checking the calculations and manuscript, and to Mr. Pierre Langevin for preparation of the drawings.

Reference

1. MOHUN, W. A. and PETERSON, W. S. Can. Chem. Process Inds. 31 : 908-913. 1947.

CANADIAN JOURNAL OF RESEARCH

VOLUME 26 DECEMBER, 1948 NUMBER 12

— SECTION F —

TECHNOLOGY

Contents

NATIONAL RESEARCH COUNCIL
OTTAWA, CANADA

CANADIAN JOURNAL OF RESEARCH

The *Canadian Journal of Research* is issued in six sections, as follows:

A. Physical Sciences	D. Zoological Sciences
B. Chemical Sciences	E. Medical Sciences
C. Botanical Sciences	F. Technology

For the present, Sections A, C, D, and E are to be issued six times annually, and Sections B and F, twelve times annually, each under separate cover, with separate pagination.

The *Canadian Journal of Research* is published by the National Research Council of Canada under authority of the Chairman of the Committee of the Privy Council on Scientific and Industrial Research. The *Canadian Journal of Research* is edited by a joint Editorial Board consisting of members of the National Research Council of Canada, the Royal Society of Canada, and the Chemical Institute of Canada.

Sections B and F of the *Canadian Journal of Research* have been chosen by the Chemical Institute of Canada as its medium of publication for scientific papers.

EDITORIAL BOARD

EDITORIAL COMMITTEE

Manuscripts should be addressed:

Editor-in-Chief,
Canadian Journal of Research,
National Research Council, Ottawa, Canada.

CANADIAN JOURNAL OF RESEARCH

Notes on the Preparation of Copy

GENERAL:—Manuscripts should be typewritten, double spaced, and the **original and one extra copy submitted.** Style, arrangement, spelling, and abbreviations should conform to the usage of this Journal. Names of all simple compounds, rather than their formulae, should be used in the text. Greek letters or unusual signs should be written plainly or explained by marginal notes. Superscripts and subscripts must be legible and carefully placed. Manuscripts should be carefully checked before being submitted, to reduce the need for changes after the type has been set. If authors require changes to be made after the type is set, they will be charged for changes that are considered to be excessive. **All pages, whether text, figures, or tables, should be numbered.**

ABSTRACT:—**An abstract of not more than about 200 words, indicating the scope of the work and the principal findings, is required.**

ILLUSTRATIONS:

(i) *Line Drawings:*—All lines should be of sufficient thickness to reproduce well. Drawings should be carefully made with India ink on white drawing paper, blue tracing linen, or co-ordinate paper **ruled in blue only**; any co-ordinate lines that are to appear in the reproduction should be ruled in black ink. Paper ruled in **green, yellow, or red should not be used** unless it is desired to have all the co-ordinate lines show. Lettering and numerals should be neatly done in India ink preferably with a stencil (**do not use typewriting**) and be of such size that they will be legible and not less than one millimeter in height when reproduced in a cut three inches wide. All experimental points should be carefully drawn with instruments. Illustrations need not be more than two or three times the size of the desired reproduction, but the ratio of height to width should conform with that of the type page. **The original drawings and one set of small but clear photographic copies are to be submitted.**

(ii) *Photographs:*—Prints should be made on glossy paper, with strong contrasts; they should be trimmed to remove all extraneous material so that essential features only are shown. Photographs should be submitted **in duplicate**; if they are to be reproduced in groups, one set should be so arranged and mounted on cardboard with rubber cement; the duplicate set should be unmounted.

(iii) *General:*—**The author's name, title of paper, and figure number should be written in the lower left hand corner (outside the illustration proper) of the sheets on which the illustrations appear.** Captions should not be written on the illustrations, but typed on a separate page of the manuscript. All figures (including each figure of the plates) should be numbered consecutively from 1 up (arabic numerals). **Each figure should be referred to in the text.** If authors desire to alter a cut, they will be charged for the new cut.

TABLES:—Titles should be given for all tables, which should be numbered in Roman numerals. Column heads should be brief and textual matter in tables confined to a minimum. **Each table should be referred to in the text.**

REFERENCES:—**These should be listed alphabetically by authors' names, numbered in that order, and placed at the end of the paper.** The form of literature citation should be that used in the respective sections of this Journal. **Titles of papers should not be given in references listed in Sections A, B, E, and F, but must be given in references listed in Sections C and D.** The first page only of the references cited in papers appearing in Sections A, B, and E should be given. **All citations should be checked with the original articles.** Each citation should be referred to in the text by means of the key number; in Sections C and D the author's name and the date of publication may be included with the key number if desired.

The *Canadian Journal of Research* conforms in general with the practice outlined in the *Canadian Government Editorial Style Manual*, published by the Department of Public Printing and Stationery, Ottawa.

Reprints

Fifty reprints of each paper without covers are supplied free. Additional reprints, if required, will be supplied according to a prescribed schedule of charges. On request, covers can be furnished at cost.